Karlsruhe Institute of Technology

Hadronisation in Herwig 7

Master's thesis of

Steffen Bengt Gay

at the Department of Physics
Institute for Theoretical Physics

Reviewer:	PD Dr. Stefan Gieseke
Second reviewer:	Prof. Dr. Dieter Zeppenfeld

12. April 2017 – 12. April 2018

Ich versichere wahrheitsgemäß, die Arbeit selbstständig verfasst, alle benutzten Hilfsmittel vollständig und genau angegeben und alles kenntlich gemacht zu haben, was aus Arbeiten anderer unverändert oder mit Abänderungen entnommen wurde sowie die Satzung des KIT zur Sicherung guter wissenschaftlicher Praxis in der jeweils gültigen Fassung beachtet zu haben.

Karlsruhe, den 12. April 2018

. . . .

(Steffen Bengt Gay)

Als Masterarbeit anerkannt.

Karlsruhe, den 12. April 2018

. . . .

(PD Dr. Stefan Gieseke)

Abstract

In this thesis the hadronisation model of Herwig 7 will be discussed and alternative approaches presented. Currently the transition in a particle collision from the high-energy regime of the hard scattering to the low-energy regime of observable particles is implemented in Herwig 7 as the cluster hadronisation model. Its main steps are cluster formation, iterative cluster fission until clusters are below a certain mass threshold and finally cluster decay into hadrons. In a first approach the iterative nature of the cluster fission is kept but the determination of the properties of the two newly produced clusters is differed. As a second approach each cluster, that is able to fission, fissions directly into a certain number of clusters which then decay into hadrons. Both approaches are explained and the results are compared to data from lepton collisions.

Contents

1 Introduction

The goal of High-Energy physics is to fundamentally understand what the universe is made of. For this purpose many particle colliders have been built over the last decades. A current example is the Large Hadron Collider (LHC) at CERN with its experiments CMS, ATLAS, ALICE and LHCb. With the discovery of the Higgs Boson at the LHC in 2012 the Standard Model (SM) is now fully discovered, yet there are phenomena which are not described by the SM. For example, with the SM itself, the existence of dark matter or the asymmetry of matter and antimatter can not be explained. Therefore, the task of the LHC and future colliders is to look for physics beyond the Standard Model (BSM).
To compare data from experiments with predictions of theory a third mainstay of physics has been playing an increasingly important role over the last decades: Simulation. With Monte Carlo event generators for example it is possible to simulate a theoretical model and get its predictions on final state distributions for a given particle collision. Monte Carlo event generators use Monte Carlo methods for numerical integration. One of these event generators is Herwig 7 [1], which is the event generator used in this thesis.
The theory of strong interaction, also known as Quantum Chromodynamics (QCD), describes the interaction of particles carrying colour charge. These can be quarks, antiquarks or gluons, collectively called partons. Particle detectors in experiments do not measure partons directly but composite particles, called hadrons, in which partons are held together by strong interaction. Theoretical models are calculated in perturbation theory. These calculations only hold true in a high energy regime. In these high energy regions partons are not bound and can move freely, called asymptotic freedom. In lower energy regions partons are confined and they form colour neutral particles, hadrons. Therefore, no colour charged particles are observed in nature and detectors in particle experiments only measure properties of colour neutral particles. For the transition from the regime of asymptotic freedom to the confinement state, perturbation theory is not a sufficient description any more. Instead one uses phenomenological models described not by a full theoretical model but by theoretical as well as experimental observations. It is therefore crucial to have models that describe data well and are based on solid theoretical considerations. The work on this thesis focuses on the hadronisation of Herwig 7, which describes the transition from free partons to excited hadrons.
For the hadronisation Herwig 7 uses the cluster model [2]. Clusters are colour singlet states formed after the parton shower from pairs of partons. Some of these clusters are too heavy to decay directly into hadrons and are therefore split into smaller clusters by sequential fissions, each into two smaller clusters, until they are below the fission threshold.
Data of most observables available is described quite well by the current hadronisation model of Herwig 7. In some regions of observables though, where hadronisation plays an important role, deviation of simulated distributions from data is up to 40% or more. Thus it is of greater interest to take a closer look at the hadronisation model, discuss its properties

and describe possible alternatives. This is the main aim of this thesis and with a better understanding of the hadronisation it aims to contribute towards a better understanding of particles and their interactions.

In the first part of this thesis the hadronisation process, its integration in the event generation as a whole and the properties of the current implementation in Herwig 7 are described. In the second part several alternative approaches to the hadronisation model will be discussed.

Chapter 2 gives a short description of QCD and its properties that form the foundation for hadronisation. For a more detailed description of QCD and the SM the reader is referred to one of the many textbooks on the topic, for example [3–5]. The following chapter gives an overview of the event generation process. In Chapter 4 the current hadronisation model is described in detail and its properties are discussed. The first alternative approach, discussed in Chapter 5, is to keep the sequential decays of one cluster into two clusters but change the way properties of these two clusters are chosen. A second alternative is introduced in Chapter 6. Here the clusters do not fission sequentially into several clusters but a cluster heavy enough to fission does so directly into a certain number of clusters which then decay into hadrons. Finally the work in this thesis is summarised and a brief outlook will be given in Chapter 7.

2 Prerequisites

The fundamental interactions between particles are described in the SM. It is a combination of two quantum field theories, QCD, and the electroweak theory. Its underlying gauge group therefore is

$$\mathrm{SU}(3)_{\mathrm{QCD}} \times \mathrm{SU}(2)_{\mathrm{L}} \times \mathrm{U}(1)_{\mathrm{Y}}. \tag{2.1}$$

The SM describes the interactions of all fundamental particles and QCD as part of the SM is the theory of the interactions between colour charged particles such as quarks and gluons. Since no bare colour charged particles are observed in nature (e.g. single quarks and gluons alone) but only particles that are neutral in terms of colour charge, a transition from the elementary process with single partons to the physically detectable particles has to be made. This transition, called hadronisation, can so far only be described by phenomenological models as perturbation theory in energy ranges $\mathcal{O}(1\ \mathrm{GeV})$ is enhanced in higher orders of the coupling constant and thus can not be truncated. The main topic of this thesis is to implement an alternative approach to the current hadronisation model in Herwig 7 [1]. As such this work builds upon the basics of QCD and its features. Therefore in this chapter there will be a short overview of QCD itself, followed by a brief summary of the relevant features for hadronisation.

2.1 Quantum chromodynamics

In this section the part of the SM that describes the interaction of quarks and gluons, namely the QCD Lagrangian, will briefly be discussed. It is based on the non-abelian gauge group SU(3) and is given by

$$\mathcal{L}_{\mathrm{QCD}} = \sum_{q=u,d,s,\ldots} \bar{q}_a (i\gamma^\mu D_\mu - m)_{ab} q_b - \frac{1}{4} F^a_{\mu\nu} F_a^{\mu\nu} + \mathcal{L}_{\mathrm{ghost}} + \mathcal{L}_{\mathrm{gauge\text{-}fixing}}, \tag{2.2}$$

where $F^a_{\mu\nu}$ is the field strength tensor given by

$$F^a_{\mu\nu} = \partial_\mu A^a_\nu - \partial_\nu A^a_\mu - g f^{abc} A^b_\mu A^c_\nu, \tag{2.3}$$

with A^a_μ being the massless gluon field with eight colour degrees of freedom and g the strong coupling constant. These gluon fields are based on the generators of the SU(3): T^a. The structure constants f^{abc} are defined in the commutation relation of the SU(3) generators

$$[T^a, T^b] = i f^{abc} T^c. \tag{2.4}$$

The covariant derivative D_μ is given by

$$D_\mu = \partial_\mu - igT^a A^a_\mu, \tag{2.5}$$

q_a are the massive quark fields in the triplet representation of the SU(3) (a = 1,2,3). The gauge fixing term $\mathcal{L}_{\text{gauge-fixing}}$ in the Lagrangian is needed to define a propagator for the gluon field A^a_μ. To cancel additional, non-physical degrees of freedom that appear because of gauge invariance, the ghost term $\mathcal{L}_{\text{ghost}}$ has to be introduced. Interaction between the massless gauge fields (here the gluon fields) and the massive quark fields is described by this covariant derivative.

2.2 Asymptotic Freedom and Confinement

In QCD the strength of the coupling α_S depends on the energy scale Q^2, at which it is considered. The running of α_S is defined by [3]

$$Q^2 \frac{\partial \alpha_S}{\partial Q^2} = \beta(\alpha_s), \tag{2.6}$$

where α_S is also dependent on the energy scale μ^2. μ^2 is the mass scale at which the subtraction in renormalisation is performed. In Eq. 2.6 the beta function can be written as the following perturbative expansion in terms of powers of α_S

$$\beta(\alpha_S) = -b\alpha_S^2(1 + b'\alpha_S + b''\alpha_S^2 + O(\alpha_S^3)), \tag{2.7}$$

with the coefficients given by

$$\begin{aligned} b &= \frac{33 - 2n_f}{12\pi}, \\ b' &= \frac{153 - 19n_f}{2\pi(33 - 2n_f)}, \\ b'' &= \frac{77139 - 15099n_f + 325n_f^2}{288\pi^2(33 - 2n_f)}, \end{aligned} \tag{2.8}$$

and n_f being the number of active flavours. Unlike b and b', which are independent of the renormalisation scheme ([3], p.36), b'' depends on the renormalisation scheme used, in this case the $\overline{\text{MS}}$ scheme [6]. If $n_f \leq 16$ the coefficients have negative signs and therefore at sufficiently large energies the coupling vanishes and partons move freely. This characteristic of QCD is called asymptotic freedom.
In the perturbative region ($Q^2, \mu^2 \gg 1$ GeV^2) for both scales μ and Q it is plausible to truncate the expansion on the right-hand side of Eq. 2.7 and neglect the term b' and terms of higher order. The solution for the coupling constant is then given by

$$\alpha_S(Q^2) = \frac{\alpha_S(\mu^2)}{1 + \alpha_S(\mu^2) b \ln\left(\frac{Q^2}{\mu^2}\right)}. \tag{2.9}$$

Since α_S cannot be calculated from the deduced equations, but rather its energy dependent behaviour, it is determined only by measurements. Usually μ^2 is set to a scale large enough to be in the perturbative regime and then deduce any other value at another scale Q^2. One common scale to measure α_S is the pole mass of the Z-boson, $M_Z = 91.2$ GeV. Current results of α_S-measurements are shown in Fig. 2.1. For $\alpha_S(M_Z) \approx 0.1181$ the running coupling constant $\alpha_S(Q^2)$ exceeds the value $\alpha_S = 1$ if $Q < \mathcal{O}(1\text{ GeV})$. This behaviour is implied in Fig. 2.1b. In this energy regime it is not sufficient any more to truncate Eq. 2.7 as the contribution of α_S increases with every order of α_S.
An alternative concept is to introduce a dimensionful parameter Λ directly into the definition of the running coupling constant

$$\alpha_S(Q^2) = \frac{1}{b \ln\left(\frac{Q^2}{\Lambda^2}\right)}. \tag{2.10}$$

Λ sets the scale at which α_S diverges and is dependent on the chosen renormalisation scheme and the order of β to which it was used in the calculation of α_S.
Over macroscopic distance scales no single quarks or gluons are observed. Therefore all colour charged particles form colour neutral states under $SU(3)_{QCD}$ at the energy scale of $\mathcal{O}(1\text{ GeV})$. This property is called confinement.

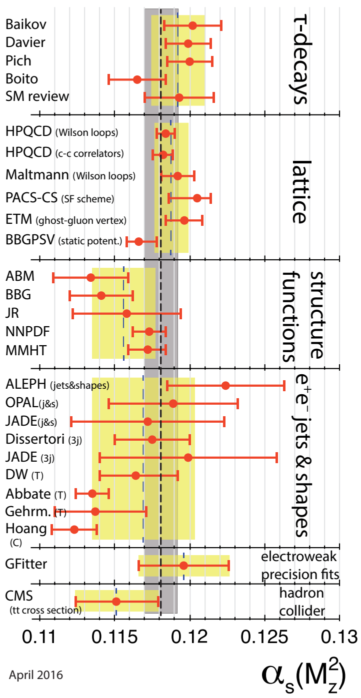

(a)

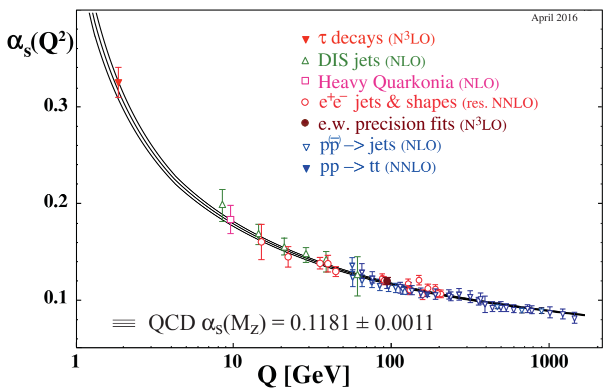

(b)

Figure 2.1: Measurements on $\alpha_S(Q^2)$ taken from [7]. On the left-hand side the mean value of several measurements of $\alpha_S(M_Z^2)$ is plotted. The energy scale μ is measured at the pole mass of the Z-boson, $M_Z = 91.2$ GeV. On the right-hand side measurements on $\alpha_S(Q^2)$ are shown.

3 Monte Carlo event generators

Monte Carlo event generators such as Herwig 7 [1, 8], Pythia 8 [9] and Sherpa 2 [10] are used to simulate high-energy particle collisions. In order to give a good description of data based on theoretical models the simulation has to cover all aspects concerning the particle collision and the transition to observable particles, measured in detectors. In Fig. 3.1 a schematic overview of a proton-proton collision is shown. The main steps are the hard scattering process, parton shower, hadronisation and hadronic decay. Incoming particles scatter at high-energy scales in the hard process. This is calculated in perturbation theory by summing over all possible Feynman-diagrams from the considered collision up to a certain order in the coupling constant. Outgoing particles from the hard scattering process are still at high-energy scales. By radiating partons in the parton shower particles reach lower energies down to the cut-off scale of the parton shower.

So far all the steps are calculated in perturbation theory. As seen in Section 2.2 at low energy scales perturbation theory falls short and therefore one has to rely on models to describe the transition from quasi-free partons to observed final state hadrons.

This chapter gives an overview of the different steps in an event simulation with Herwig 7. Starting with a brief description of the physics behind the hard scattering process, afterwards the different approaches to simulating the parton shower will be described. Next the hadronisation will be briefly outlined, followed by an explanation of underlying events and finally hadronic decays.

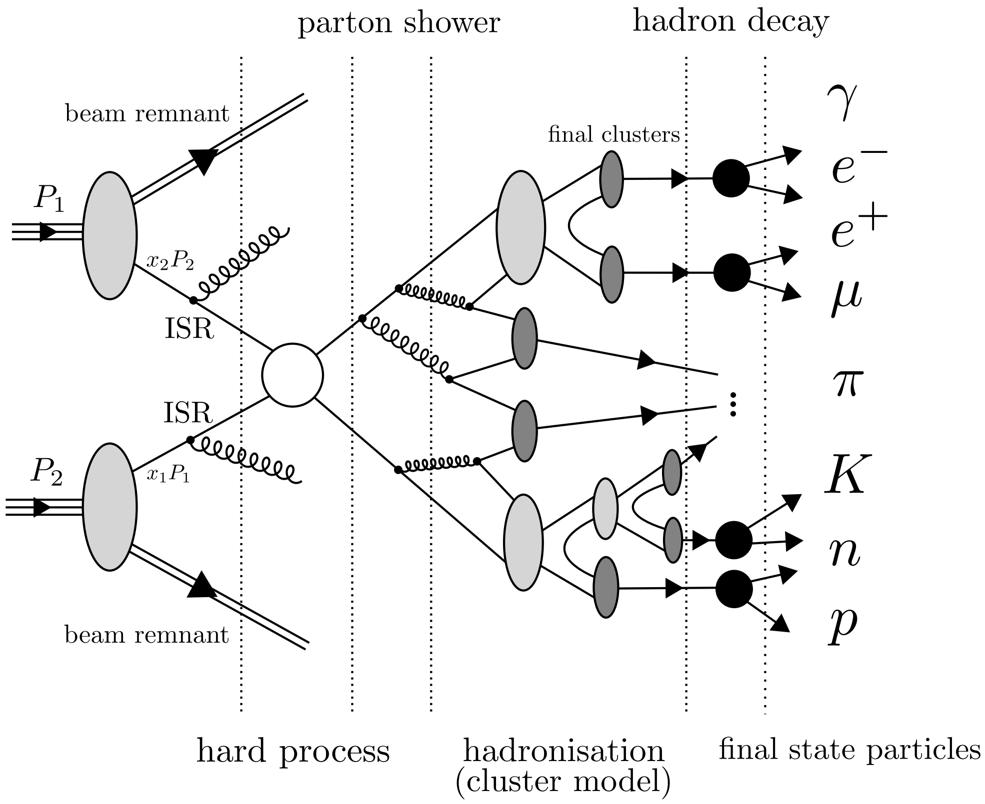

Figure 3.1: Overview of a Monte Carlo event simulation. Shown is a collision of two protons with momenta P_1 and P_2. In this case two partons scatter at momentum fractions x_1P_1 and x_2P_2 producing two new fundamental primary particles. The incoming partons might radiate additional gluons, this is called initial state radiation (ISR). After the hard process the energy of these partons gets scaled down to the hadronic scale by radiating new partons. In the hadronisation the partons in the final state of the parton shower get clustered together to form excited states of hadrons. In the final step the excited hadrons decay into the observed final state particles.

3.1 Hard scattering process

Particle collisions are categorised depending on the type of the colliding particles, e.g. hadron-hadron collision, lepton-lepton collision. This is important for the hard scattering process insofar as hadrons are composite particles and resulting collisions in the hard scattering processes therefore depend on the exact structure of incoming hadrons. For incoming leptons this is not the case as leptons are so far understood as fundamental particles. The cross section of a hard scattering process is given by [3]

$$\sigma(P_1, P_2) = \sum_{i,j} \int_0^1 dx_1 dx_2 f_i(x_1, \mu_F) f_j(x_2, \mu_F) \hat{\sigma}_{ij}(p_1, p_2, \alpha_s(\mu_F), Q^2/\mu_F). \tag{3.1}$$

To take the hadron composition into account $f_{i,j}(x_{1,2}, \mu_F)$ has to be used in the cross section calculation. $f_{i,j}(x_{1,2}, \mu_F)$ is the parton distribution function (PDF), the probability to find a certain parton i or j inside the hadron with momentum fraction $x_{1,2}$ at energy scale μ_F. The parton entering the hard scattering process therefore has momentum equal to the momentum fraction $p_{1,2} = x_{1,2}P_{1,2}$. For parton collisions the cross section $\hat{\sigma}_{ij}(p_1, p_2, \alpha_s(\mu_F), Q^2/\mu_F)$ is given by

$$\hat{\sigma}_{ij} = \int \mathrm{d}\Phi_n \frac{1}{2s} |\mathcal{M}_{ij \to n}|^2 (\Phi_n; \mu_F, \mu_R). \tag{3.2}$$

For a given parton-parton collision all possible configurations of Feynman-diagrams are summed and squared in the squared matrix element $|\mathcal{M}_{ij\to n}|^2(\Phi_n; \mu_F, \mu_R)$. Lastly, $d\Phi_n$ is the differential phase space element for an n-particle final state.
Calculating the hard cross section therefore relies on PDFs provided by several external collaborations. Herwig 7 has built-in PDFs that can be used, additional PDFs can be accessed via LHAPDF [11]. For the actual calculations of Feynman diagrams in the hard scattering process Herwig 7 can calculate some built-in matrix elements. For additional matrix elements external matrix element providers such as MADGRAPH [12] and VBFNLO [13–15] can be used. The resulting particles are then forwarded to the parton shower discussed in the following section.

3.2 Parton shower

The hard scattering process can be calculated in QCD up to next-to-leading order (NLO) in α_s as a whole and only in parts up to next-to-next-to-leading order (NNLO) in α_s. Since higher order corrections cannot be neglected in certain regions of phase space an additional approach to include higher order corrections has to be taken into account when simulating whole events.
The parton shower is such an approach that takes effects of all orders into account. Starting from the energy scale of the hard process Q^2 the parton shower evolves particles down to the evolution cut-off scale Q_0^2, usually $\sim 1\ \mathrm{GeV}^2$. In this section at first the basic outlines of the parton shower algorithm will be explained followed by a short clarification on the differences regarding the parton shower algorithm for initial and final states. The section is concluded by a short exposition of the two shower algorithms implemented in Herwig 7.

3.2.1 Final state evolution

Following the description of the parton shower basics from Ref. [16] closely the shower is firstly described for $e^+e^- \to q\bar{q}g$ and then generalised for any process. At first the cross section $\sigma_{e^+e^-\to q\bar{q}g}$ is formulated in such a way that it is given by $\sigma_{e^+e^-\to q\bar{q}}$ with an additional gluon emission. The differential cross section $\mathrm{d}\sigma_{q\bar{q}g}$ is given by

$$\frac{\mathrm{d}\sigma_{q\bar{q}g}}{\mathrm{d}\cos\theta \mathrm{d}z} \approx \sigma_{q\bar{q}} C_F \frac{\alpha_s}{2\pi} \frac{2}{\sin^2\theta} \frac{1 + (1-z)^2}{z}, \tag{3.3}$$

where θ is the opening angle between the gluon and the quark, z is the energy fraction of the gluon and $C_F = \frac{N_c^2-1}{2N_C}$ is the colour factor. In Eq. 3.3 all the non divergent terms were neglected, so that the divergences occurring are:

- $\theta \to 0$, the collinear limit, where the gluon is emitted in the same direction as the quark momentum direction.
- $\theta \to \pi$, where the gluon is emitted collinear to the antiquark.
- $z \to 0$, where the energy of the emitted gluon goes to zero independent of the opening angle.

For the following consideration only the first two divergences in the collinear region are considered.
The angular distribution can be separated into two components so that only one of the two components diverges at the corresponding collinear region. With $\bar{\theta}$ being the angle between the gluon and the antiquark the angular distribution is expressed by

$$\frac{2}{\sin^2\theta} \approx \frac{1}{1-\cos\theta} + \frac{1}{1-\cos\bar{\theta}}. \tag{3.4}$$

This separation then corresponds to

$$\mathrm{d}\sigma_{q\bar{q}g} \approx \sigma_{q\bar{q}} \sum_{\text{partons}} C_F \frac{\alpha_s}{2\pi}\frac{\mathrm{d}\theta^2}{\theta^2}\mathrm{d}z\frac{1+(1-z)^2}{z}, \tag{3.5}$$

where now θ is the opening angle between the gluon and the emitting parton. In Eq. 3.5 the differential cross section is given by the sum of the independent emissions from the quark and antiquark. This structure is completely general and can therefore be expressed for any hard process as

$$\mathrm{d}\sigma \approx \sigma_0 \sum_{\text{partons},i} \frac{\alpha_s}{2\pi}\frac{\mathrm{d}\theta^2}{\theta^2}\mathrm{d}zP_{ji}(z,\phi)\mathrm{d}\phi. \tag{3.6}$$

Here the cross section σ_0 describes a hard process that produces partons of flavour i, emitting a parton j which has momentum fraction z. P_{ij} are spin- and flavour-dependent splitting functions and are given for the spin average by

$$P_{qq}(z) = C_F\frac{1+z^2}{1-z}, \qquad P_{gq}(z) = C_F\frac{1+(1-z)^2}{z} \tag{3.7}$$

$$P_{gg}(z) = C_A\frac{z^4+1+(1-z)^4}{z(1-z)}, \quad P_{qg}(z) = T_R(z^2+(1-z)^2). \tag{3.8}$$

C_F, C_A and T_R are colour factors, where T_R is defined as $T_R = \frac{1}{2}$.
Before deriving an actual iterative algorithm where one can use Eq. 3.6 iteratively the still existing divergences have to be taken care of. Since exactly collinear partons, that have the same total momentum and other quantum numbers, cannot be physically distinguished, a resolution criteria should be introduced. One choice of a resolution criteria is the transverse momentum, so that two partons are resolvable if their relative transverse momentum is above the cut-off scale Q_0^2. With this, both the collinear and the soft divergences are taken care of and the total resolvable emission probability is finite.

For all branchings of a certain parton i the total probability distribution in the energy range between q^2 and $q^2 + \mathrm{d}q^2$ is

$$\mathrm{d}\mathcal{P}_i = \frac{\alpha_s}{2\pi}\frac{\mathrm{d}q^2}{q^2}\int_{Q_0^2/q^2}^{1-Q_0^2/q^2} \mathrm{d}z P_{ji}(z), \tag{3.9}$$

where q^2 is the virtuality of the internal quark propagator and the limits on z result from the condition that the partons are resolvable. To get the probability distribution of the first branching at q^2 one needs to first calculate the probability that there was no branching at a scale higher than q^2. This probability is defined as $\Delta_i(Q^2, q^2)$ and is known as the Sudakov form factor. It is given by the differential equation

$$\frac{\mathrm{d}\Delta_i(Q^2, q^2)}{\mathrm{d}q^2} = \Delta_i(Q^2, q^2)\frac{\mathrm{d}\mathcal{P}_i}{\mathrm{d}q^2}, \tag{3.10}$$

where the solution is

$$\Delta_i(Q^2, q^2) = \exp\left(-\int_{q^2}^{Q^2}\frac{\mathrm{d}k^2}{k^2}\frac{\alpha_s}{2\pi}\int_{Q_0^2/k^2}^{1-Q_0^2/k^2} \mathrm{d}z P_{ji}(z)\right). \tag{3.11}$$

The upper limit Q^2 is the maximum possible virtuality. With the Sudakov form factor it is now possible to formulate an iterative algorithm suitable for a Monte Carlo implementation. One possible implementation is as follows. Firstly a random number $\mathcal{R}(0;1)$ is chosen, then the equation

$$\Delta_i(Q^2, q^2) = \mathcal{R} \tag{3.12}$$

is solved for q^2. If the solution is above the cut-off scale Q_0^2 the branching is generated and z is calculated from $P_{ij}(z)$. For each branching product the steps are repeated until the resulting $q^2 < Q_0^2$ i.e. no more emissions can be resolved.

3.2.2 Initial state evolution

So far only particles produced in the hard process were taken into account of the shower algorithm. However particles before the hard scattering process are able to shower off just as much. Simply applying the final state evolution to incoming particles and using appropriate particles from the shower's final state is extremely inefficient as the probability of the partons having the correct kinematics for a specific hard process is very small [16]. What is done instead is to select the wanted hard process at first and generate the additional radiation (initial and final) around it.

For the initial state radiation the Sudakov form factor from Eq. 3.11 is replaced by

$$\Delta_i(Q^2, q^2; x) = \exp\left(-\int_{q^2}^{Q^2}\frac{\mathrm{d}k^2}{k^2}\frac{\alpha_s}{2\pi}\int_{Q_0^2/k^2}^{1-Q_0^2/k^2} \mathrm{d}z P_{ij}(z)\frac{\frac{x}{z}f_j\left(\frac{x}{z}, k^2\right)}{x f_i(x, k^2)}\right), \tag{3.13}$$

which now depends explicitly on the PDFs of the incoming hadrons and the momentum fraction x. A consequence of the ratio of the two PDFs in Eq. 3.13 is that for increasing x the PDF decreases and the emission probability will be small. It is therefore more likely that the parton came directly from the hadron, being a valence quark, than resulting from an evolution of a higher-x-parton.

3.2.3 Shower algorithms

In Herwig 7 two different shower algorithms are implemented. The default algorithm is the angular ordered $\widetilde{q}$-shower [17]. Additionaly, the dipole shower algorithm is implemented [18, 19].

3.2.3.1 Angular ordered shower

The basis for the angular ordered shower algorithm is the coherent branching algorithm. It preserves angular ordering and provides invariance under boosts along the jet axis [17]. The cross section for a soft gluon emission contains the dipole radiation terms [20]

$$W_{ij}(k) \equiv \omega^2 \left(\frac{p_i \cdot p_j}{(p_i \cdot k)(p_j \cdot k)} - \frac{1}{2} \frac{p_i^2}{(p_i \cdot k)^2} - \frac{1}{2} \frac{p_j^2}{(p_j \cdot k)^2} \right), \tag{3.14}$$

where p_i and p_j are the momenta of the colour connected partons and k is the momentum of the radiated gluon. The angles between the directions of particles i,j and k are labelled θ_{ij}, θ_{ik}, etc. For $\theta_{ik} \to 0$ or $\theta_{jk} \to 0$ Eq. 3.14 contains collinear singularities and can be rewritten as

$$W_{ij}(k) \equiv W_{ij}^{(i)}(k) + W_{ij}^{(j)}(k). \tag{3.15}$$

$W_{ij}^{(i)}$ contains a collinear singularity only for $\vec{k}$ parallel to $\vec{p}_i$ and not for $\vec{k}$ parallel to $\vec{p}_j$, therefore it is associated with the gluon emission off parton i. Furthermore it is given by [20]

$$W_{ij}^{(i)}(k) = \frac{\beta_i}{2\zeta_{ik}} \left(\frac{\beta_i - \cos\theta_{ik}}{1 - \beta_i \cos\theta_{ik}} + \frac{\cos\theta_{ik} - \beta_j \cos\theta_{ij}}{1 - \beta_j (\cos\theta_{ij} \cos\theta_{ik} + \sin\theta_{ij} \sin\theta_{ik} \cos\phi_i)} \right), \tag{3.16}$$

where ϕ_i is the azimuthal angle w.r.t. $\vec{p}_i$ and $\beta_i = \frac{v_i}{c}$. Eq. 3.16 is positive-definite for $\theta_{ik} < \theta_{ij}$. For $\theta_{ik} > \theta_{ij}$ the function can have negative values, resulting in destructive interference. The azimuthal average, given by [20]

$$\langle W_{ij}^{(i)} \rangle_{\phi_i} = \frac{\beta_i}{2\zeta_{ik}} \left(\frac{\beta_i - \cos\theta_{ik}}{(1 - \beta_i \cos\theta_{ik})} + \frac{\cos\theta_{ik} - \beta_j \cos\theta_{ij}}{\sqrt{|\cos\theta_{ik} - \beta_j \cos\theta_{ij}|^2 + (1 - \beta_j^2) \sin^2\theta_{ik}}} \right), \tag{3.17}$$

is in the massless limit, $\beta_{i,j} \to 1$, the Heavyside step-function $\Theta(\theta_{ij} - \theta_{ik})$. To have a resulting soft radiation the opening angle θ_{ik} therefore has to be smaller than θ_{ij}, this is the angular ordering property.

In shower algorithms the partons exiting the hard process and initiating the shower are called shower progenitors. The scaling variable for the angular ordered shower in Herwig 7 for the evolution of partons with space-like virtualities is written in terms of the respective opening angles as

$$\widetilde{q}^2 = \frac{2E_a(1 - \cos\theta_{bc})(1 + \cos\theta_a)^2}{(1 + \cos\theta_b)(1 + \cos\theta_c)}. \tag{3.18}$$

Where, considering the branching $a \to b + c$, θ_a is the angle between the parent particle and the progenitor. θ_b, θ_c are the angles between the children particles b, c and the progenitor. For small emission angles the evolution variable is given by

$$\widetilde{q} = E_a \theta_{bc} (1 - \mathcal{O}(\theta_x^2)). \tag{3.19}$$

For every branching the children partons with momentum fractions z and, because of four-momentum conservation, $1 - z$ have the starting evolution scale at $z\widetilde{q}$ and $(1 - z)\widetilde{q}$

$$\begin{aligned} z\widetilde{q} &\approx E_a \theta_{bc}, \\ (1 - z)\widetilde{q} &\approx E_b \theta_{bc}. \end{aligned} \tag{3.20}$$

The maximum opening angle of a following branching is θ_{bc}, therefore in any subsequent branching the branching angle is smaller than θ_{bc}.

3.2.3.2 Dipole shower

The dipole shower model is based on Catani-Seymor subtraction kernels [21]. In the limit of large N_c, where N_c is the number of colours, the colour structure of the parton shower can be drawn on a plane like the one shown in Fig. 3.2, where colour-anticolour partners are aligned adjacent to each other. Every colour line connecting two partons forms a colour-anticolour dipole. In the soft-gluon and large-N_C limit each of these dipoles emits independently. This emission is carried out recursively until a certain cut-off is reached and the shower is terminated. Gluons carry colour lines of two dipoles and so dipole radiations involving gluons may affect the subsequent radiation pattern of neighbouring dipoles. The recoil in systems with finite transverse momenta affects both dipoles connected to the gluon. To prevent this, the shower is evolved globally and the dipole emission with the highest transverse momentum emission is generated first to set the upper limit for the subsequent evolution. Since in the case of dipole showering emissions are $2 \to 3$ processes instead of $1 \to 2$ processes, four-momentum can be explicitly conserved at every step in the shower.

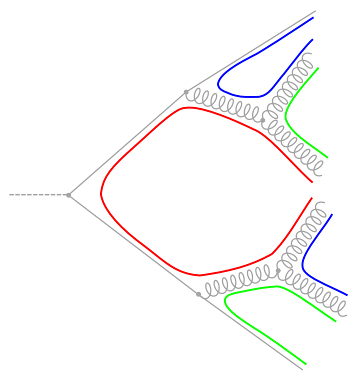

Figure 3.2: Planar representation of the colour structure of a parton shower in the limit of large N_c.

3.3 Hadronisation, brief outline

To convert the partons from the parton shower into hadrons different models are used by the different MC event generators. In Pythia the Lund-String model [22] is used whereas Herwig 7 uses the cluster model [2]. The cluster model, initially proposed by Wolfram and Field [2], is based on the preconfinement property of the angular ordered parton shower [23, 24]. Preconfinement states, that pairs of colour-connected partons close to each other in space-time can be arranged into colour singlet states. These colour singlet states have an asymptotic mass distribution which is independent of the hard process scale and the properties of the parton shower.
Gluons left by the parton shower are split non-perturbatively into quark-antiquark pairs. From all the remaining quarks and antiquarks colour neutral clusters are formed. These clusters then either decay into hadrons directly or, if too heavy, fission iteratively into additional clusters until the mass of the clusters reaches a certain mass cut-off scale. For the sake of completeness it should be noted that the constituents of a cluster do not necessarily have to be (anti-)quarks but can also be so called (anti-)diquarks. (Anti-)Diquarks, two (anti-)quarks grouped together, play a role when there are beam remnants involved in the process. Since this thesis focuses solely on lepton collisions, (anti-)diquarks are not considered any further. The hadronisation process is described in detail in Chapter 4.

3.4 Underlying event

In hadron colliders not only the primary hard process and its subsequent steps contribute to the event but also other processes involving the remnants of incoming hadrons. All elementary particles involved in hadron collisions are colour charged and can therefore interact with each other. In experiments every interaction except for the hard process of interest is defined as an underlying event, therefore underlying events are not limited to soft interactions (interactions with low p_T) but also involve hard interactions (interactions with high p_T).
In Herwig 7 the default model for the underlying event is a model for multiple parton interactions (MPIs) which is based on the eikonal model [25–27]. There are two parts in the model, a perturbative and a non-perturbative part [28], which are separated depending on the transverse momentum. If the interactions are above a certain p_T^{min} MPIs are modelled as QCD $2 \to 2$ processes, called semihard interactions. On the other hand, if the interactions are below p_T^{min} they are modelled as elastic gluon scattering, called soft interactions.
With the release of Herwig 7.1 a new model to describe these soft interactions is introduced as the default model [29]. Instead of producing a gluon pair for each soft interaction a number of gluons, determined by a Poisson distribution, and a pair of quarks is produced. The gluons produced are restricted to the regime of soft transverse momenta $p_T < p_T^{min}$ and are ordered in rapidity, resulting in a "roughly flat distribution in rapidity of the clusters and the subsequently produced particles" ([30], p.5). This leads to major improvements in describing data which was insufficiently described before [30]. Similar kinematics will be used in the "1 to N"-model later on in this thesis as an alternative approach to cluster fission with sequential two body decays.

3.5 Cluster and hadron decays

Once all heavy clusters are fissioned into smaller clusters the clusters then decay into pairs of excited hadrons. The hadrons produced are selected from all possible flavours depending on the available phase space, the spin and the flavour of the cluster's constituents.
Once the decay products are chosen the hadrons are isotropically distributed in the cluster rest frame. If a hadron contains a parton, produced in the perturbative stage of the event, the direction of this parton is kept except for a small change in direction with a gaussian smearing. The smearing angle θ_{smear} is randomly chosen according to

$$\cos\theta_{\text{smear}} = 1 + \mathbf{CL}_{\text{smear}} \log\mathcal{R}, \tag{3.21}$$

where $\mathbf{CL}_{\text{smear}}$ is a free parameter dependent on the flavour of the parton. The azimuthal angle relative to the parton direction is chosen randomly following a uniform distribution from 0 to 2π.
If a cluster is too light to decay into a pair of hadrons it decays directly into a hadron with appropriate flavour. To allow the correct physical mass of this hadron, energy and momentum are reshuffled with the neighbouring clusters in a small range. As a final step the excited hadrons then decay into final state particles that can be seen in detectors.

4 Hadronisation

As the work in this thesis solely focuses on discussing alternatives to the current hadronisation of Herwig 7 the following chapter will give a closer overview of this model. After a description of the sequential steps in the hadronisation, the impact of current hadronisation parameters is shown followed by a discussion of the limits when describing data with the current model.

4.1 Gluon splitting and cluster formation

The partons handed over to the hadronisation by the parton shower can be quarks or gluons. The first step of the hadronisation is to split all the received gluons into quark-antiquark pairs, then the remaining partons will be combined into colour neutral clusters. As can be seen in Fig. 4.1 quark-antiquark pairs (or under special circumstances diquarks-antidiquark pairs) sharing the same colour line will be combined into the same cluster.

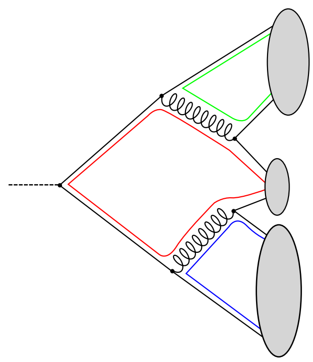

Figure 4.1: Gluon splitting and cluster formation.

4.2 Cluster Fission

Most of the newly formed clusters then decay into hadrons directly. Some of the clusters do not decay directly into hadrons but split up into new clusters, this splitting is called cluster fission. The purpose of this recursive non perturbative fission process is the transition from particles with higher energy to a greater number of particles with lower energy. This effect can be seen in Fig. 4.2. For a cluster to fission, its mass has to fulfil the inequality

$$M^{Cl_{\text{pow}}} \geq Cl_{\text{max}}^{Cl_{\text{pow}}} + (m_1 + m_2)^{Cl_{\text{pow}}}, \tag{4.1}$$

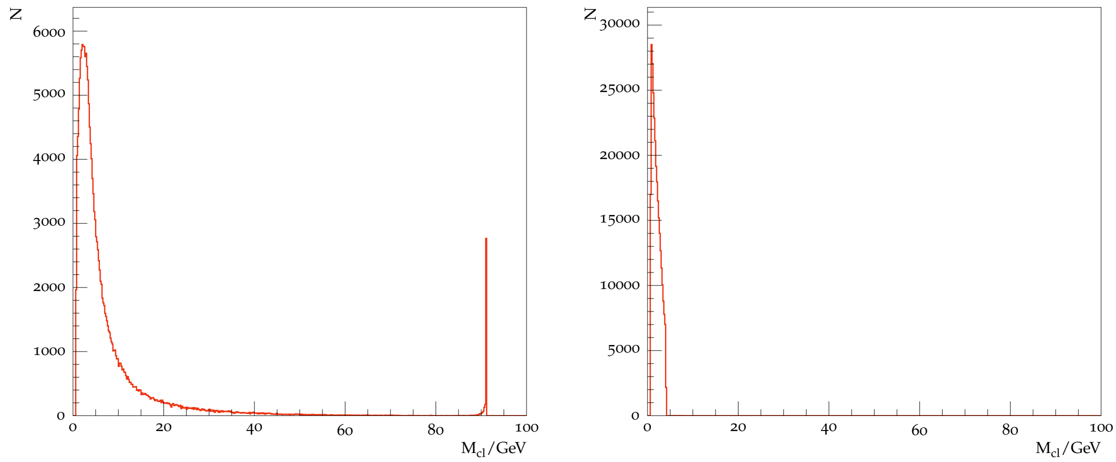

(a) (b)

Figure 4.2: Mass distribution for the default mass sampling of the process $e^+e^- \to jj$ with the leading order default shower, ISR and colour reconnection turned on. In Fig. (a) the masses of primary clusters are shown. They result from either the parton shower or the hard process (peak at $M_{cl} = 91.2$ GeV). In Fig. (b) the masses of all remaining clusters, after cluster fission was applied, are shown. The effect of the cluster fission is clearly visible as it shifts all clusters to lower masses and produces additional clusters.

where M is the cluster's mass and $m_{1,2}$ are the constituent masses of the cluster. Cl_{pow} and Cl_{max} are free parameters to control the threshold at which clusters fission. Both parameters depend on the flavour of the cluster's constituents and are therefore different for clusters containing light (up, down), charm, etc. quarks. As can be seen in Fig. 4.3 the parent cluster, with two constituents, fissions into two new clusters. During the fissioning process a quark-antiquark pair is produced from the vacuum. Each of the two children clusters gets one constituent of the parent cluster and the matching quark or antiquark from the vacuum. The probability of producing a quark-antiquark pair with a specific flavour is controlled by the parameter Pwt. The masses of the new clusters

$$
\begin{aligned}
M_1 &= m_1 + \mathcal{R}_1^{\frac{1}{P_{\text{split}}}}, \\
M_2 &= m_2 + \mathcal{R}_2^{\frac{1}{P_{\text{split}}}},
\end{aligned}
\tag{4.2}
$$

depend on the mass of the parent cluster M, the masses of the parent cluster's constituents $m_{1,2}$, the masses of the produced quark-antiquark pair $m_{q,\bar{q}}$ and on one of the random numbers $\mathcal{R}_{1,2}$. $\mathcal{R}_{1,2}$ are uniformly distributed random numbers between $m_{q,\bar{q}}$ and $(M - m_1 - m_2 - m_{q,\bar{q}})$ taken to the power of P_{split},

$$
\begin{aligned}
&\mathcal{R}_1\left(m_q^{P_{\text{split}}}; (M - m_1 - m_2 - m_q)^{P_{\text{split}}}\right)^{\frac{1}{P_{\text{split}}}}, \\
&\mathcal{R}_2\left(m_{\bar{q}}^{P_{\text{split}}}; (M - m_1 - m_2 - m_{\bar{q}})^{P_{\text{split}}}\right)^{\frac{1}{P_{\text{split}}}}.
\end{aligned}
\tag{4.3}
$$

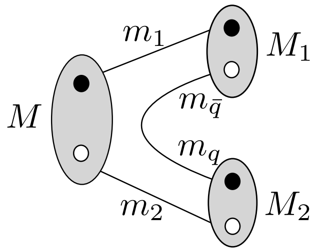

Figure 4.3: Cluster fission.

Additionally there are constraints on the masses of the fissioned clusters. The sum of the masses of the children clusters is required to be less than the mass of the parent cluster and the mass of each cluster is supposed to be greater than the sum of the masses of its constituents.
A short overview of the parameters is given in Table 4.1.

Table 4.1: Description of parameters in the default cluster fission model.

Parameter	Description
ClMaxLight, *ClMaxBottom*, *ClMaxCharm*	Set the threshold mass for clusters to fission.
ClPowLight, *ClPowBottom*, *ClPowCharm*	Set the exponent for the threshold mass for clusters to fission.
PwtDquark, *PwtUquark*, *PwtSquark*, *PwtDIquark*	Set the weight for choosing a specific flavour.
PSplitLight, *PSplitBottom*, *PSplitCharm*	Control the mass region of M_1 and M_2.

4.3 Discussion of the current hadronisation model

While some observables are very well described by the current hadronisation model in Herwig 7, other observables are not well described and particularly in certain regions. As of now the main dataset to tune and compare hadronisation effects of event generators to is data from the Large-Electron-Positron collider (LEP). Therefore in this thesis if not explicitly stated otherwise the process used for simulation is $e^+e^- \to q\bar{q}$, where only light flavours are considered, at a centre of mass energy of 91.2 GeV and data is taken from the DELPHI experiment [31].
One very well described observable is the mean charged multiplicity which can be seen in Fig. 4.5a. All tested parton shower and matching methods are within 5% deviation from data. In Fig. 4.5b the number of produced particles over the scaled momentum x_p is plotted. It is defined as the momentum of a single particle scaled to the momentum of the beam

$$x_p = \frac{|\vec{p}|}{|\vec{p}_{beam}|}. \tag{4.4}$$

For low momentum fractions the data is well described. However, for scaled momenta close to $x_p = 1$ the number of particles produced in simulations varies significantly from data in the order of 40% deviation.
The thrust, defined as

$$T = \max_{\vec{n}_{\text{thrust}}} \frac{\sum_{i=1}^{N_{\text{particle}}} |\vec{p}_i \cdot \vec{n}_{\text{thrust}}|}{\sum_{i=1}^{N_{\text{particle}}} |\vec{p}_i|}, \tag{4.5}$$

is a shape variable, describing the spreading of outgoing particles in an event. $\vec{p}_i$ are the momenta of all final state hadrons in the event and $\vec{n}_{\text{thrust}}$ is an arbitrary unit vector. $\vec{n}_{\text{thrust}}$ points in the direction that maximises T. If $T \approx 1$ the outgoing particles are spatially distributed close to each other. In this region hadronisation plays a superior role as there is little radiation and therefore the kinematics, i.e. the transverse momentum, are mainly described by hadronisation. For the opposite, $T = \frac{1}{2}$, the outgoing particles are spread across all spatial direction and the event is spherically shaped. Here hadronisation plays an important role as well as fixed order calculations can not be used, but kinematics are mainly determined by radiation. For a given thrust T the shape of an event can further be determined by the thrust major M. It is defined as

$$M = \max_{\vec{n}_M} \frac{\sum_{i=1}^{N_{\text{particle}}} |\vec{p}_i \cdot \vec{n}_M|}{\sum_{i=1}^{N_{\text{particle}}} |\vec{p}_i|}. \tag{4.6}$$

Where $\vec{n}_M$ is a unit vector perpendicular to the thrust axis $\vec{n}_{\text{thrust}}$ pointing in the direction that maximises M. Together with the thrust minor m, whose axis $\vec{n}_m$ is perpendicular to both the thrust axis and the thrust major axis, the three axes define the shape of a cone. As shown in Fig. 4.4, the thrust axis $\vec{n}_T$ points in the direction of the cone, the thrust major axis $\vec{n}_M$ points in the direction of the big half axis and the thrust minor $\vec{n}_m$ points in the direction of the small half axis. In both border regions of the thrust observable simulation

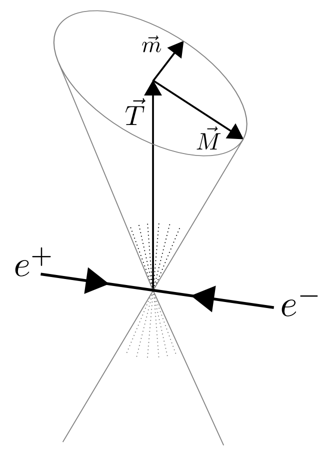

Figure 4.4: Direction of thrust, thrust major and thrust minor axis in a particle collision, where $\vec{T} = T \cdot \vec{n}_{\text{thrust}}$, $\vec{M} = M \cdot \vec{n}_M$ and $\vec{m} = m \cdot \vec{n}_m$.

does not agree with data very well, which can be seen in Fig. 4.5c where not the thrust

itself but the difference $1 - T$ is shown. Similar behaviour can be seen for the thrust major M in Fig. 4.5d. Description from simulation of both observables differs up to more than 40% from data in referred regions.
In Fig. 4.6 some characteristic distributions for clusters in the current default model of Herwig 7 are shown. Fig. 4.6a and Fig. 4.6d show the masses of all occuring clusters. The peak at 91.2 GeV in Fig. 4.6a is the mass of all the initial clusters and in Fig. 4.6d it is the mass of initial clusters in those events where the parton shower did not produce additional gluons. The shift in masses and therefore the shift in energy from the parton shower cut-off scale to the scale of observable hadrons is also visible in both Fig. 4.6a and 4.6d as the peak at low masses comes solely from final clusters and everything in between is from clusters that are neither initial clusters nor final clusters. Fig. 4.6b and Fig. 4.6e show that clusters have in general low transverse momenta. In Fig. 4.6c and Fig. 4.6f the rapidity distributions are shown. Rapidity is defined as

$$y = \frac{1}{2} \ln \left(\frac{E + p_z}{E - p_z} \right), \tag{4.7}$$

where a z-direction is chosen (in most cases the beam direction), p_z is the component of the particle momentum in that direction and E is the energy of the considered particle. The rapidity is an interesting observable for collider experiments as its distribution is invariant under boosts along the chosen z-axis, as well as differences in rapidity ([7], p. 562). Cluster fission on its own produces mostly clusters with smaller rapidities but almost no clusters with rapidities of around $y = 0$. With the parton shower turned on, more clusters with higher momentum transverse to the beam axis are produced. Therefore more clusters with rapidity $y = 0$ are produced compared to events with the parton shower turned off.
To see the impact of hadronisation on the observables discussed before and shown in Fig. 4.5 the main parameter of the current default model, *PsplitLight*, is varied and the output compared to data. In Fig. 4.7a the mean charged multiplicity is shown on which the variation of *PsplitLight* has significant effects as the deviation of some runs from data is more than 40%. The same can be said for high scaled momentum $x_p > 0.2$ and low scaled momentum $x_p < 0.05$ shown in Fig. 4.7b. For the thrust T and the thrust major M deviation stays mostly within ≈40%, see Fig. 4.7c and Fig. 4.7d. In regions discussed before, high and low thrust $(1 - T) \to \{0.5, 0\}$ as well as high and low thrust major $M \to \{0.5, 0\}$, differences between the runs are significantly large.
The variation shows that in regions where data of depicted observables is not well described hadronisation plays an important role as it influences these distributions significantly. Therefore to improve agreement with data it is of interest to take a closer look at the hadronisation model used in Herwig 7. As described in Sec. 4.2 the properties of the newly produced clusters mainly depend on the sampling parameters which control the mass sampling in the cluster fission. In the following chapter the presented alternatives keep the main structure of the cluster fission as sequential two body decays but the process of sampling the cluster masses is changed. Whether or not these alternative approaches are an improvement is not clear right away and therefore they will be discussed in the subsequent chapter.

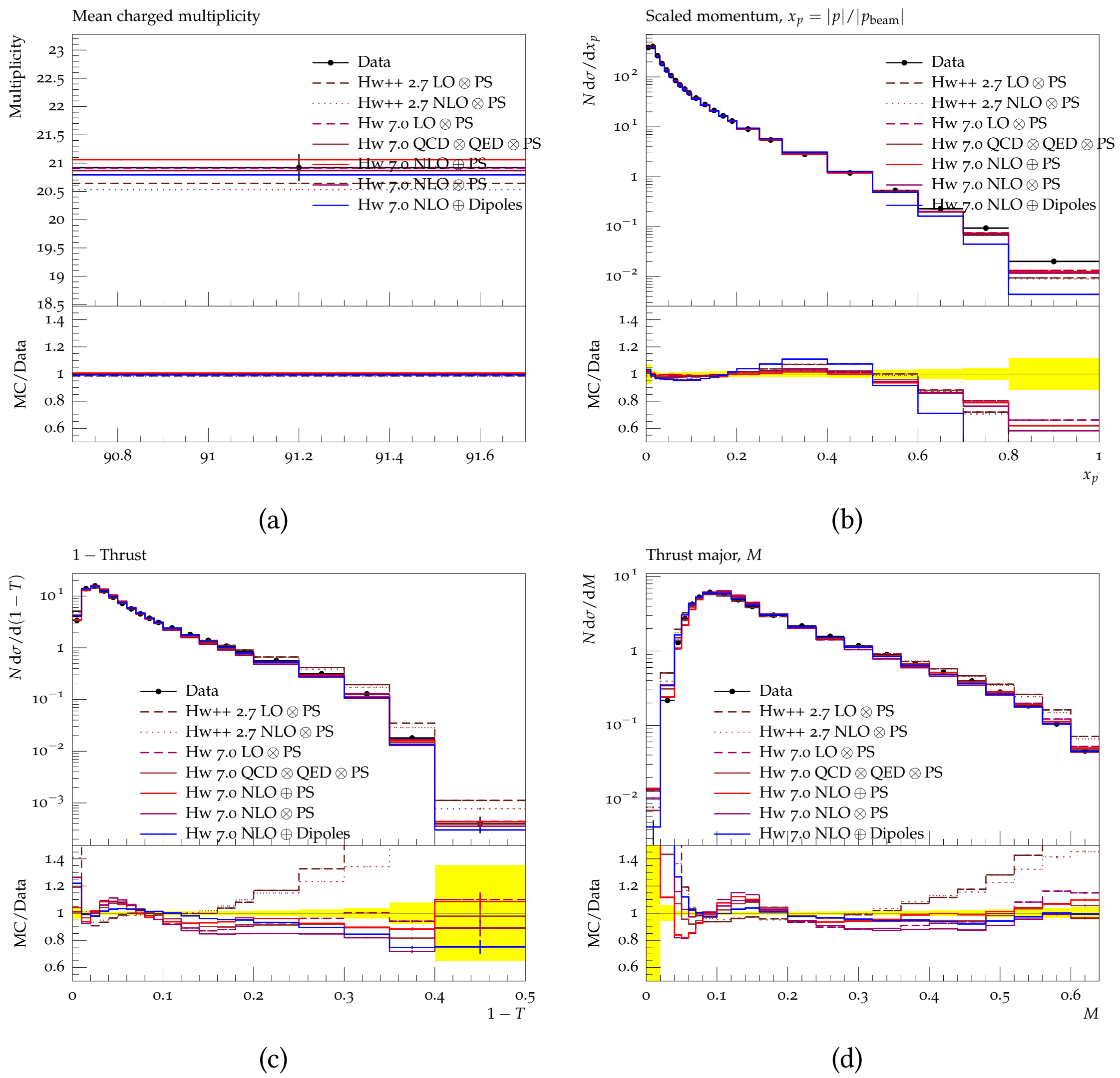

Figure 4.5: Comparison with data of observable distributions for different settings of Herwig 7/Herwig++ [1, 8], different parton shower algorithms and matching methods, taken from [32]. In the plots ⊕ stands for MC@NLO being used as a matching method and ⊗ for POWHEG being used.

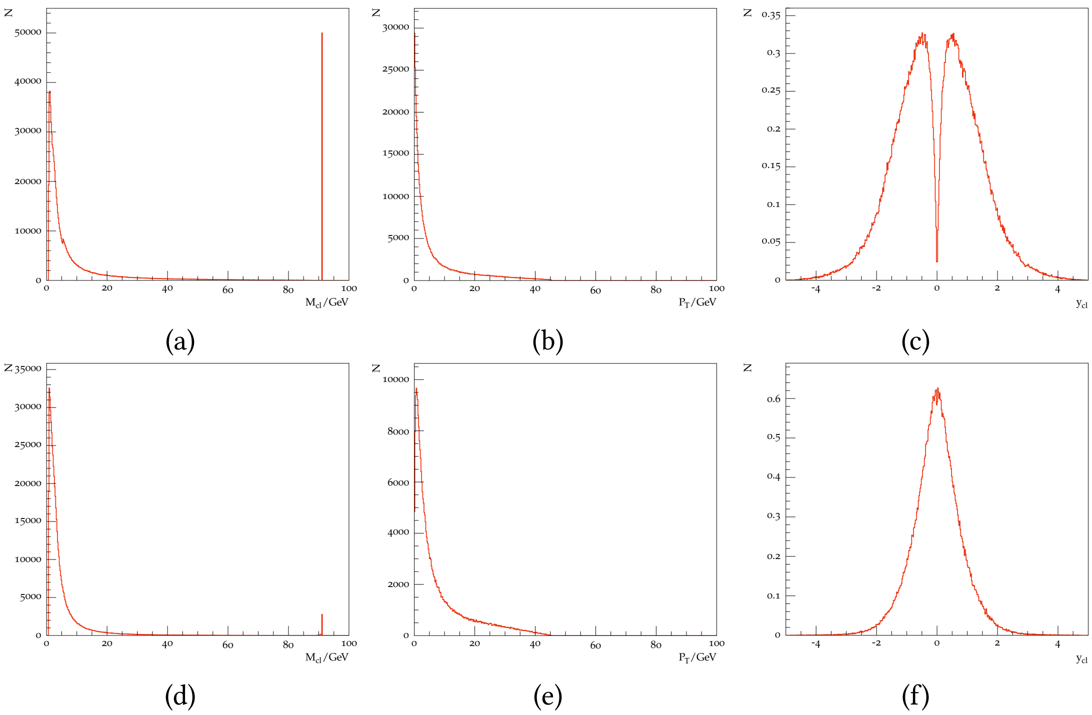

Figure 4.6: Distributions for $e^+e^- \to jj$ at centre of mass energy 91.2 GeV.(a)-(c) are from runs without ISR, colour reconnection and parton shower. (d)-(f) are from runs with ISR, colour reconnection and the LO-defaultshower turned on. (a)&(d) show the masses of all clusters in the events, (b)&(e) show the transverse momenta p_T of final clusters and (c)&(f) show the rapidity of final clusters.

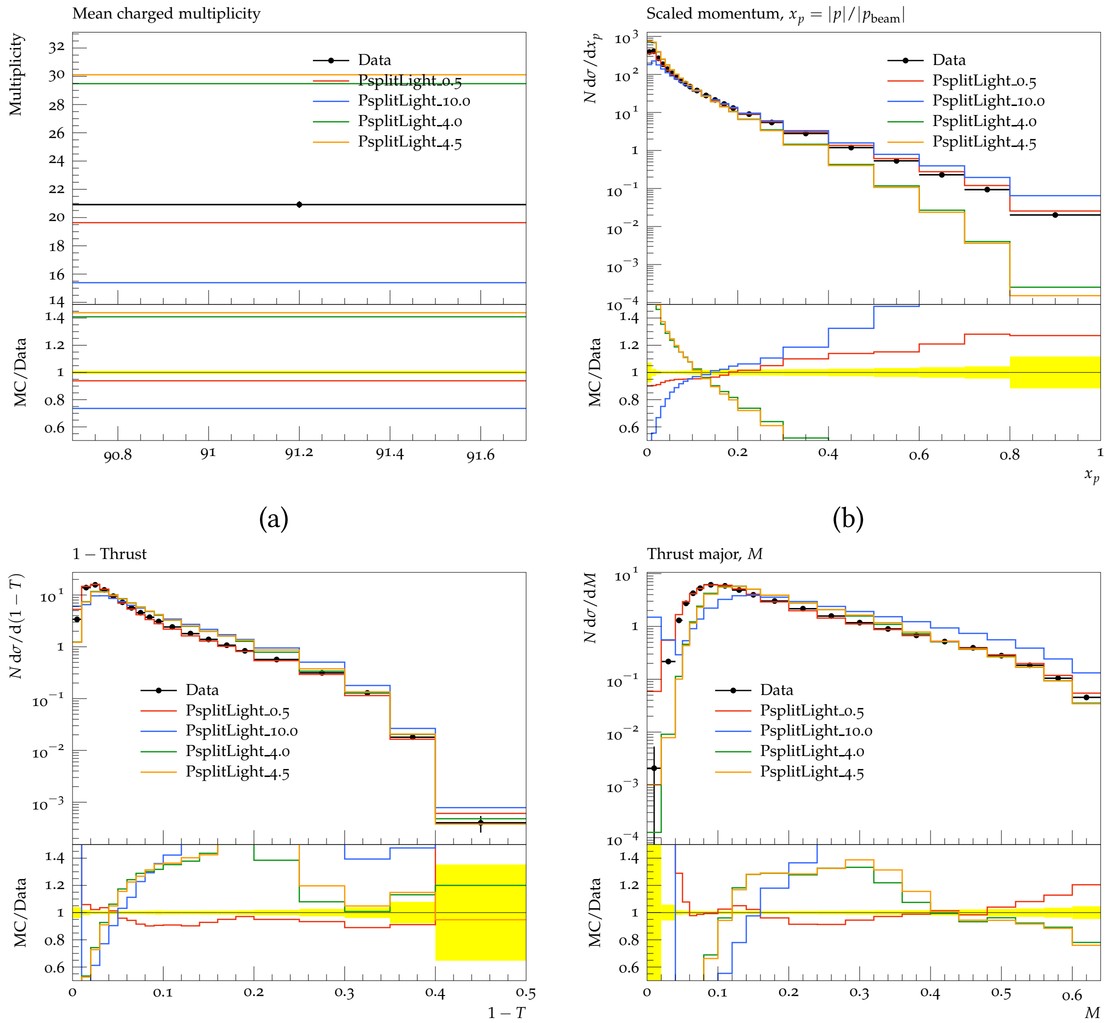

(c) (d)

Figure 4.7: Observable distributions [31] compared to runs with variation of P_{split}. The simulated process is $e^+e^- \to q_{\text{light}}\bar{q}_{\text{light}}$ at a centre of mass energy of 91.2 GeV with ISR, colour reconnection and the LO-defaultshower turned on. In this case only *PsplitLight*, the parameter for light flavoured quarks, is varied while P_{split} for the other flavours is fixed at the default values.

5 Cluster Fission via rapidity sampling

As a first approach instead of sampling the masses of clusters the rapidities of the clusters will be sampled. The kinematics of the produced clusters can then be determined from their rapidities. Since the following approaches were mostly examined in the bachelor's thesis by Maximilian Horzela [33] this chapter will give an enhanced overview without going into too much detail. A first description is given of the basic equations for the kinematics of the clusters and constraints on sampling. Thereafter, several different probability density functions for sampling the rapidities are examined and compared. Finally, a comparison is made between the new sampling approaches and their relative performance is discussed.

5.1 Basic kinematics

In the centre of mass frame of the fissioning cluster with mass M the rapidity defined in Eq. 4.7 for each of the two outgoing particles with mass M_1 and M_2 can be rewritten as

$$\begin{aligned} y_1 &= \log\left(\frac{\sqrt{M_1^2 + p^{*2}} + p^*}{M_1}\right), \\ y_2 &= -\log\left(\frac{\sqrt{M_2^2 + p^{*2}} + p^*}{M_2}\right), \\ p^* &= \frac{\sqrt{M^4 + M_1^4 + M_2^4 - 2M_1^2M_2^2 - 2M^2M_1^2 - 2M^2M_2^2}}{2M}. \end{aligned} \tag{5.1}$$

Where p^* is introduced to shorten the equation and four momentum conservation in the centre of mass frame of the fissioning cluster is used. With the rapidities defined in the centre of mass frame of the fissioning cluster it is also possible to describe the fissioning process in terms of a relative rapidity Δy and a centre of mass rapidity y^*, given by

$$\begin{aligned} \Delta y &= \frac{y_1 - y_2}{2}, \\ y^* &= \frac{y_1 + y_2}{2}. \end{aligned} \tag{5.2}$$

5.1.1 Constraints on rapidity

When sampling the rapidities not all rapidity values are accepted as there still are constraints on the masses for example. From the constraints on cluster masses defined in

Section 4.2, rapidity constraints can be directly derived.
If both children clusters share each half the parent cluster's mass then the rapidity is

$$y_{1_{\min}} = y_{2_{\min}} = 0, \tag{5.3}$$

which is therefore the minimal absolute value for rapidities. On the other hand the maximal values of the rapidities are reached when the cluster masses are minimal. This is the case when

$$\begin{aligned} M_1 &= m_1 + m_q, \\ M_2 &= m_2 + m_{\bar{q}}, \end{aligned} \tag{5.4}$$

so the cluster masses are solely given by the sum of their constituent masses.
Constraints on the centre of mass rapidity and the relative rapidity result from constraints on the individual rapidities

$$\begin{aligned} |\Delta y|_{\min} &= 0, \\ |y^*|_{\min} &= 0, \\ |\Delta y|_{\max} &= \frac{y_{1_{\max}} + y_{2_{\max}}}{2}, \\ |y^*|_{\max} &= \max(y_{1_{\max}}, y_{2_{\max}}). \end{aligned} \tag{5.5}$$

As derived in [33] by inverting Eq. 5.2 the cluster masses dependent on Δy and y^* are given by

$$\begin{aligned} M_1 &= \frac{M \cdot \sinh(\Delta y - y^*)}{\sinh(2\Delta y)}, \\ M_2 &= \frac{M \cdot \sinh(\Delta y + y^*)}{\sinh(2\Delta y)}. \end{aligned} \tag{5.6}$$

Likewise the same can be done with Eq. 5.1 to get the masses from the sampled rapidities

$$\begin{aligned} M_1 &= -M \cdot \operatorname{csch}(y_1 - y_2) \cdot \sinh(y_2), \\ M_2 &= M \cdot \operatorname{csch}(y_1 - y_2) \cdot \sinh(y_1). \end{aligned} \tag{5.7}$$

The corresponding phase space in rapidity is shown in Fig. 5.1. Since the children clusters fly off back to back their rapidities must have an opposite sign. Therefore the rapidities can have values in only two quadrants, namely quadrant II and IV, as seen in Fig. 5.1a and Fig. 5.1b. An additional constraint is derived from the fact that cluster masses are always at least given by the sum of their constituents' masses or higher. This can be seen in Fig. 5.1a and Fig. 5.1b along the rounded edges for low mass (dark blue area) and high values of the rapidities plotted on the abscissa. So not all values of y_1 and y_2 are allowed, with the boundaries defined in Eq. 5.5. In addition to the different signs of the rapidities the lower mass bound of clusters also has to be taken into account when sampling the rapidities. It proved to be sufficient to calculate the masses from generated rapidities and immediately veto out fission processes whose rapidities fail mass constraints. The available phase space for Δy and y^* is shown in Fig. 5.1c and Fig. 5.1d where the same constraints on masses and consequently on rapidities are applied.

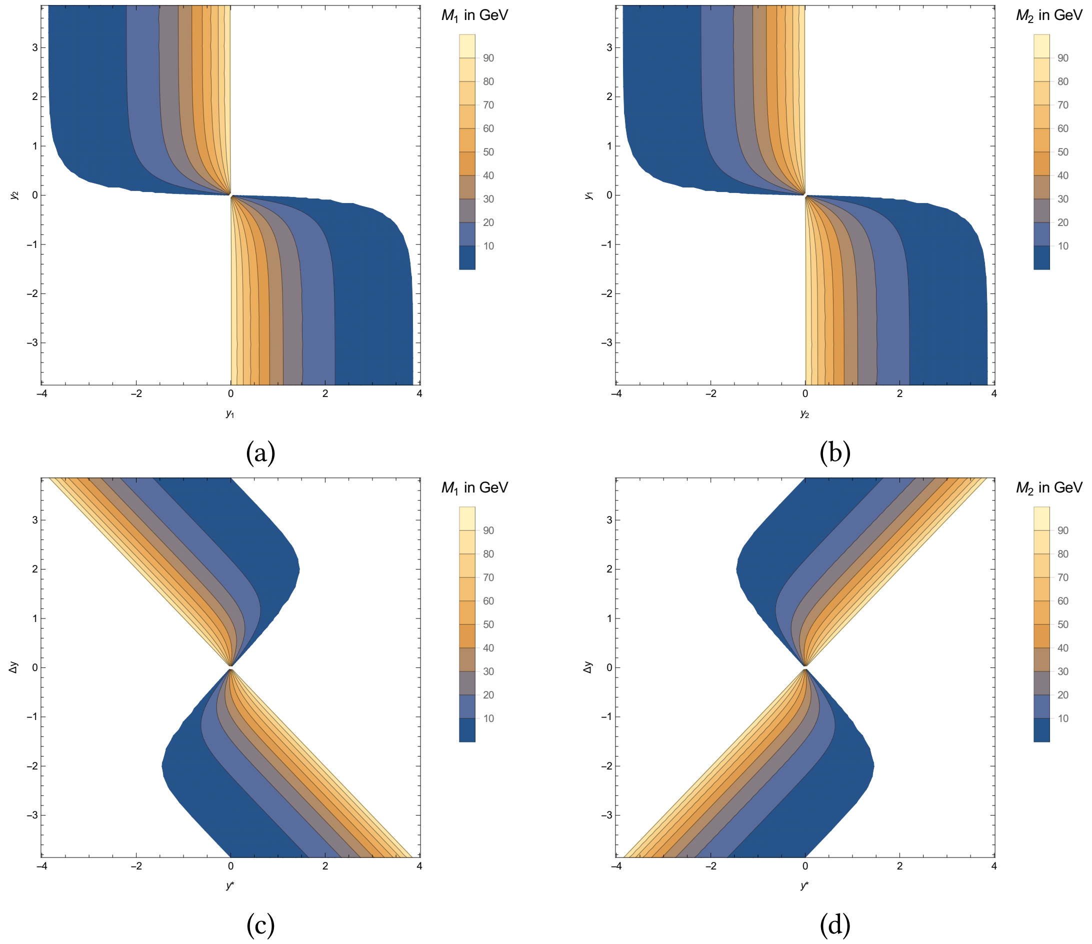

Figure 5.1: In (a), (b) possible regions to sample y_1 and y_2, depending on M_1 and M_2, are shown. Since both clusters fly off back to back there are only two quadrants in the y_1-y_2-plane rapidities can be sampled from. With the additional constraint that both children clusters have to have a minimal mass of at least the sum of their constituents the edges for higher rapidities are rounded. In (c), (d) possible regions to sample Δy and y^*, depending on M_1 and M_2, are shown. Constraints are still that both clusters fly off back to back and have at least the mass of the sum of their constituents. Analogue to Figs. (a) and (b) only half the Δy-y^*-plane minus the reduction from the minimal mass constraint can be sampled from.

5.2 Sampling by power law

Following the sampling procedure for the cluster masses the first approach is to sample Δy and y^* according to a power law. Therefore a uniformly distributed random number $\mathcal{R}$ between 0 and Δy_{max} or respectively 0 and y^*_{max} taken to the power of an exponent is drawn. The actual rapidities are then given by

$$\Delta y = \pm\mathcal{R}\left(0; |\Delta y|_{\max}^{\alpha_{pow}}\right)^{\frac{1}{\alpha_{pow}}}, \tag{5.8}$$

$$y^* = \pm\mathcal{R}\left(0; |y^*|_{\max}^{\beta_{pow}}\right)^{\frac{1}{\beta_{pow}}}, \tag{5.9}$$

where the signs are chosen randomly but with equal probabilities. To avoid divergences in the case of exponent values smaller than one and rapidity values in the limit to zero an additional parameter, e.g. δ, should be introduced to shift the boundaries by the value of δ [33].

5.2.1 Results

To get a feeling for the new sampling method the boundaries of the new parameters have to be tested. Unlike the default sampling method which has only one parameter for sampling the masses two parameters are now introduced. Therefore, in this subsection which is only a brief look at the properties of the new sampling method one parameter is fixed and the other is varied.
Runs for different parameter values compared with LEP data on LEP observables are shown in Fig. 5.2 and Fig. 5.3. As mentioned in Chapter 4.3 the mean charged multiplicity is well described by the current model. Therefore every newly introduced model has to describe the mean charged multiplicity as well as the current model does.
In both variations the mean charged multiplicity data is either not described by the runs with the specific parameter settings, see Fig. 5.2b and Fig. 5.3b, or described by just the boundary values of the parameters , see Fig. 5.2a and Fig. 5.3a. In regions of higher values of T, meaning $1 - T \approx 0$, power law sampling does not improve agreement with data and is not able to describe data within the examined parameter range. The same argument is valid for values of $1 - T > 0.2$, shown in Figs. 5.2c, 5.2d and Figs. 5.3c, 5.3d. Additionally, description of the scaled momentum x_p, shown in Figs. 5.2e, 5.2f and Figs. 5.3e, 5.3f, does not seem to be improved by a power sampling approach of Δy and y^*.
In some regions of the observables discussed above data is not even within the reach of the parameter values. Thus, tuning the newly introduced parameters to data does not seem to be of use. Therefore, other possible approaches to sample Δy and y^* will be examined in the following sections.

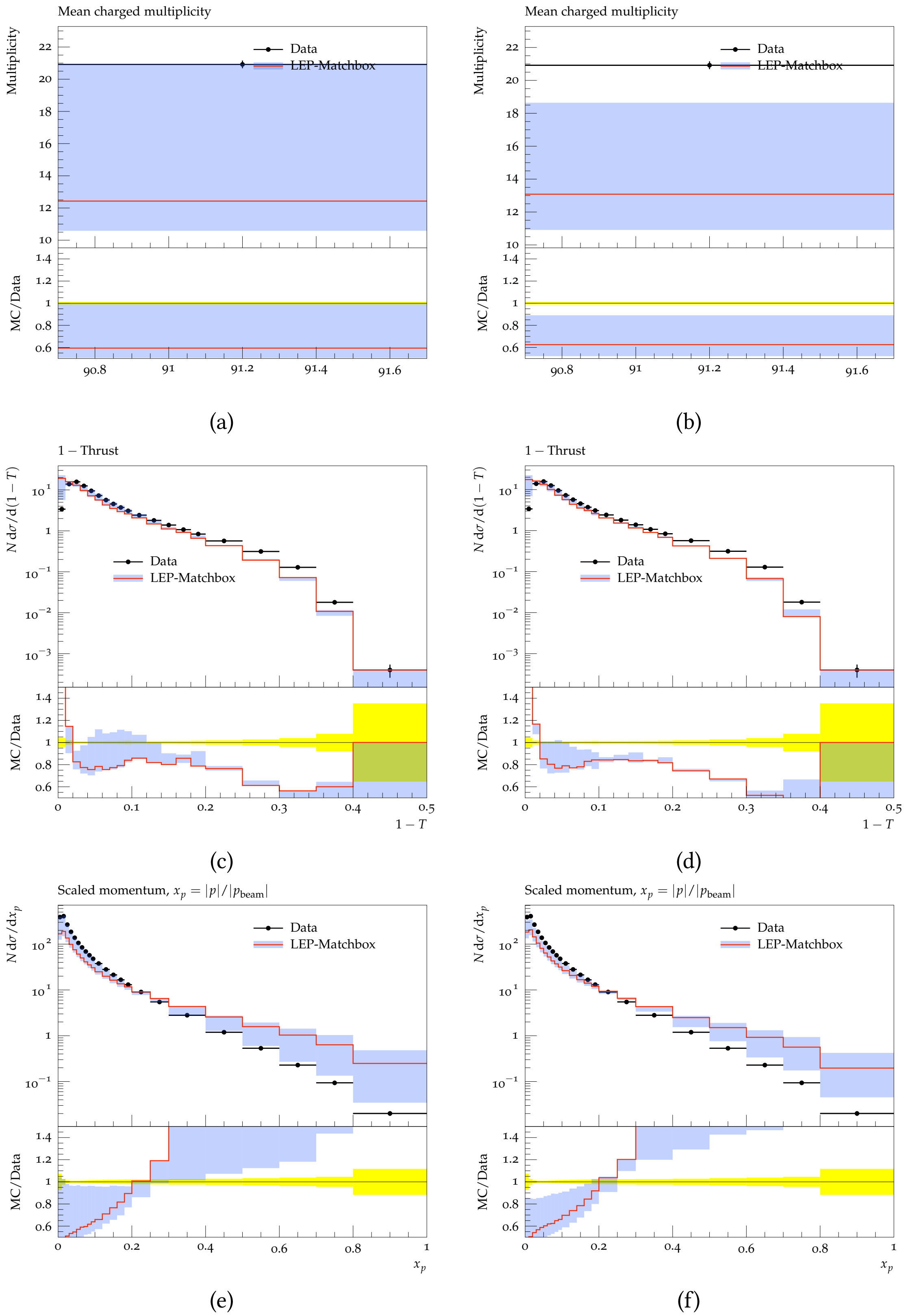

Figure 5.2: Possible regions of observables [31] sampling Δy and y^* according to a power law. β_{pow} is fixed at $\beta_{pow} = 0.1$ (left) and $\beta_{pow} = 1.0$ (right). α_{pow} is varied from $\alpha_{pow} = 0.1$ to $\alpha_{pow} = 15.0$. The red line indicates runs with $\alpha_{pow} = 4.0$.

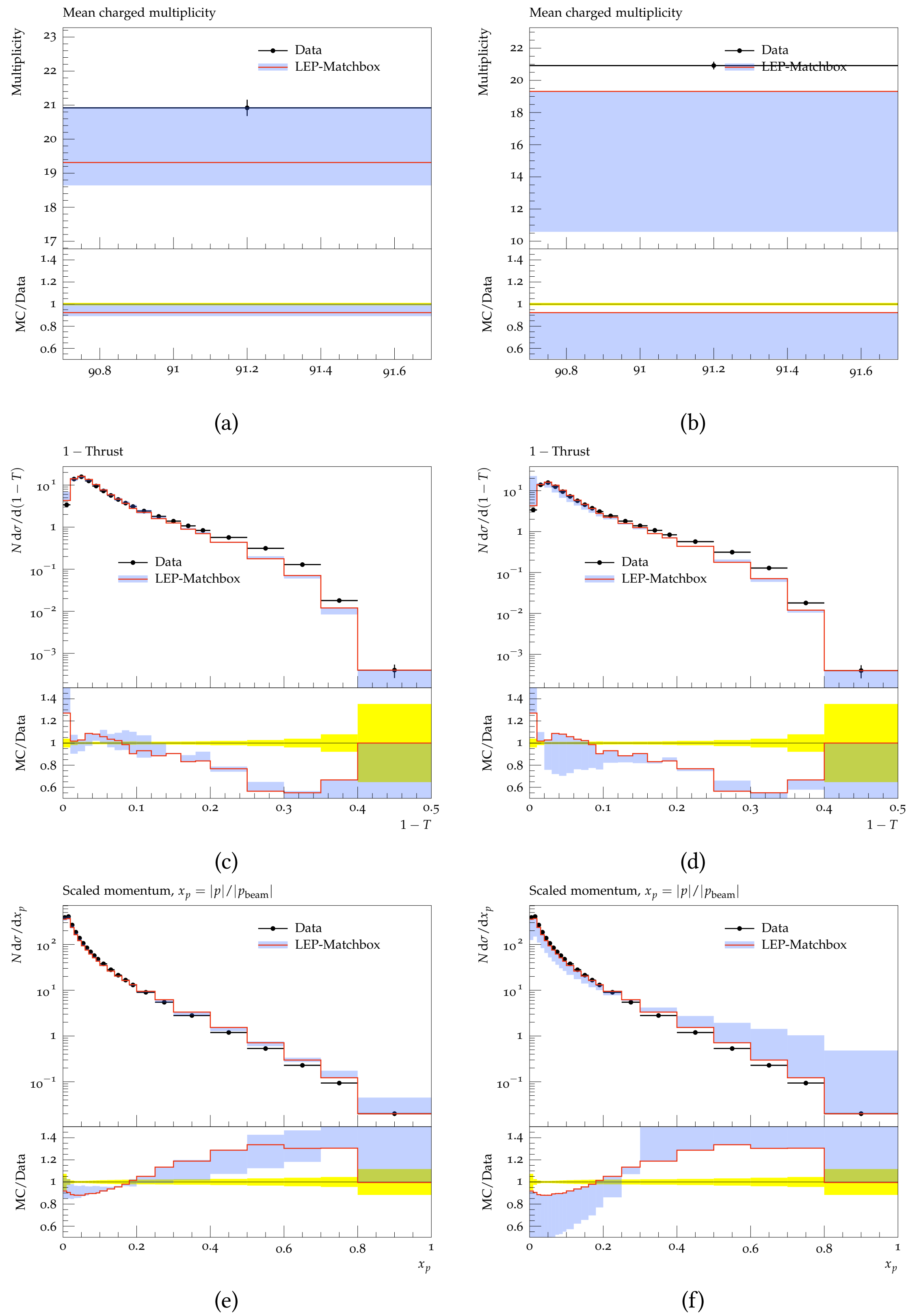

Figure 5.3: Possible regions of observables [31] sampling Δy and y^* according to a power law. α_{pow} is fixed at $\alpha_{pow} = 0.1$ (left) and $\alpha_{pow} = 15.0$ (right). β_{pow} is varied from $\beta_{pow} = 0.1$ to $\beta_{pow} = 1.0$. The red line indicates runs with default sampling and tuned parameters in this case.

5.3 Sampling by exponential law

Sampling Δy and y^* according to a power law produces less massive clusters and fewer clusters at smaller Δy [33]. Therefore a probability density function with steeper decline for higher values of Δy and y^* is needed. An exponential distribution,

$$f(x) = \lambda e^{-\lambda x}, \tag{5.10}$$

does exactly that which is why in this section sampling according to an exponential distribution will be examined. Like in the two previous approaches a cluster fissions into two clusters and their properties, in this case rapidities, are sampled randomly. For each Δy and y^* uniformly distributed random numbers $\mathcal{R}$ are drawn from 1 to the exponent of either Δy_{max} or y^*_{max}. To manipulate the distribution two new parameters are introduced analogously to the power law sampling method. Both rapidities are then given by

$$\begin{aligned} \Delta y &= \pm \frac{1}{\alpha_{exp}} \ln \left(\mathcal{R} \left(1; e^{-\alpha_{exp} |\Delta y|_{\max}} \right) \right), \\ y^* &= \pm \frac{1}{\beta_{exp}} \ln \left(\mathcal{R} \left(1; e^{-\beta_{exp} |y^*|_{\max}} \right) \right). \end{aligned} \tag{5.11}$$

5.3.1 Results

For this sampling method two parameters are introduced. One parameter is fixed while the other is varied analogously to the discussion of the power law sampling method. The number of final clusters over their rapidity relative to the momentum direction of the constituents of the primary cluster is plotted in Fig. 5.4. For $\alpha_{exp} = 0.3$ and $\beta_{exp} = 5.0$ there is a plateau in rapidity between $y \approx \pm 2$, which is an interesting distribution of clusters because commonly physics in soft energy regions is uniformly distributed in rapidity. But it is also clear from Fig. 5.4 that the distribution does not seem to be very stable as for small changes in α_{exp}, shown in Fig. 5.4a, and β_{exp}, shown in Fig. 5.4b, the shape of the distribution changes significantly.

Fixing β_{exp} and varying α_{exp} produces a more uniform distribution of rapidity so the following discussion will focus on that case. With this approach, data of the mean charged multiplicity is well within reach of the parameter range as can be seen in Fig. 5.5a and is therefore not immediately ruled out. The same can be said about about the scaled momentum x_p (Fig. 5.5b), the thrust $1 - T$ (Fig. 5.5c) and mostly the thrust major M (Fig. 5.5d) distributions. For values of M higher than $M = 0.58$ the parameter range does not describe data. The instability of the rapidity distributions is also clearly visible in the observable distributions as certain bands for the available parameter range are large. In some regions, namely x_p higher than 0.6 or $1 - T$ higher than 0.3, the band of possible values is several magnitudes wide.

As a consequence of the instability of the rapidity distributions and the observable distributions it does not seem to be reasonable to attempt further tuning of parameters for this model. Hence, the exponential law approach is dropped as an alternative to the current model and alternative probability density distributions are (briefly) tested.

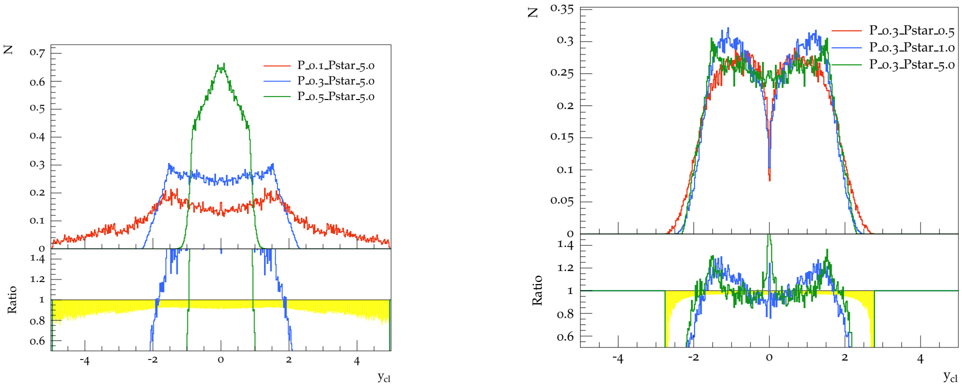

(a) (b)

Figure 5.4: The number of clusters in the final state before decaying into hadrons plotted over rapidity relative to the momentum axis of the parent cluster's constituents for different values of α_{exp} and β_{exp}. In (a) β_{exp} is fixed at $\beta_{exp} = 5.0$ and α_{exp} is varied from $\alpha_{exp} = 0.1$ to $\alpha_{exp} = 0.5$. In (b) $\alpha_{exp} = 0.3$ and β_{exp} is varied from $\beta_{exp} = 0.5$ to $\beta_{exp} = 5.0$.

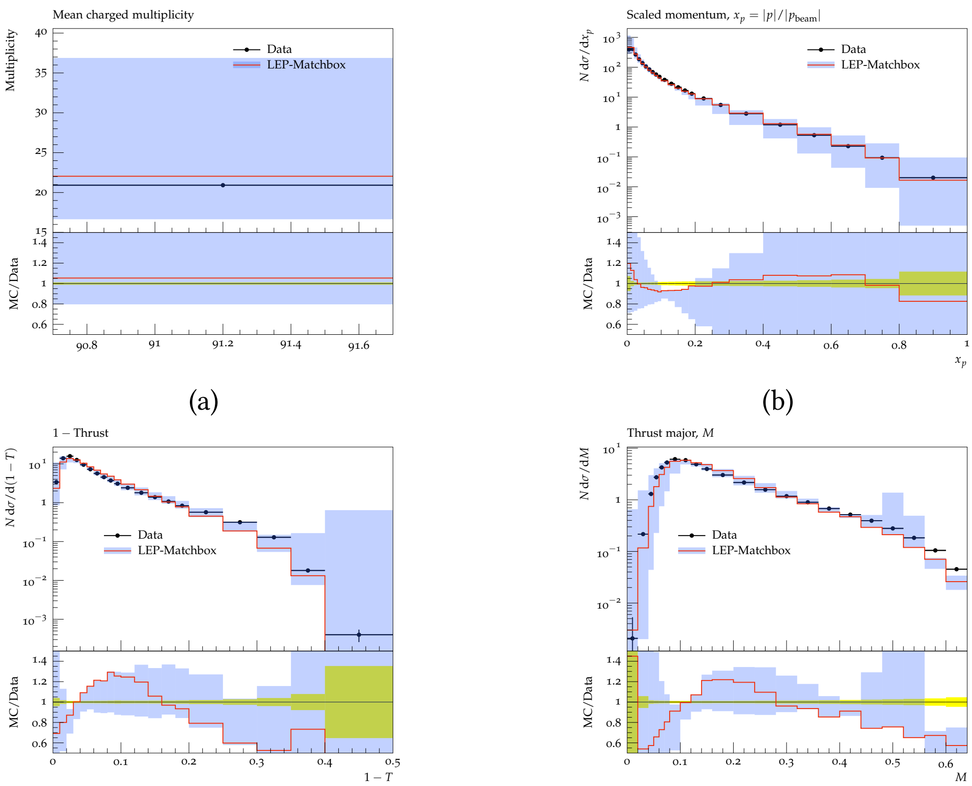

(a) (b) (c) (d)

Figure 5.5: Possible regions of observables [31] sampling Δy and y^* according to exponential law. β_{exp} is fixed at $\beta_{exp} = 5.0$ and α_{exp} is varied from $\alpha_{exp} = 0.1$ to $\alpha_{exp} = 1.0$. The red line indicates runs with $\alpha_{exp} = 0.3$.

5.4 Sampling by different density functions

So far only Δy and y^* were sampled with two different probability density distributions. To fully test rapidity sampling the rapidities of the children clusters, y_1 and y_2, are now sampled directly. Firstly, y_1 and y_2 will be sampled according to a power law, analogously to the sampling of Δy and y^*. In this case only one parameter is introduced, so that the rapidities are given by

$$y_1 = \pm\mathcal{R}\left(0; y_{1_{\max}}^{P_{split}}\right)^{\frac{1}{P_{split}}}, \tag{5.12}$$

$$y_2 = \pm\mathcal{R}\left(0; y_{2_{\max}}^{P_{split}}\right)^{\frac{1}{P_{split}}}, \tag{5.13}$$

with P_{split} acting in the same way as for the mass sampling in the current model. For values of P_{split} where the rapidity distribution seems to form a plateau there is always a dip in the number of final clusters. This is the case for low rapidities above $P_{split} = 0.5$ as can be seen in Fig. 5.6. Because of this a second approach to sampling y_1 and y_2 is considered. The second approach is to sample both rapidities following a mixed distribution of an exponential and a power law.

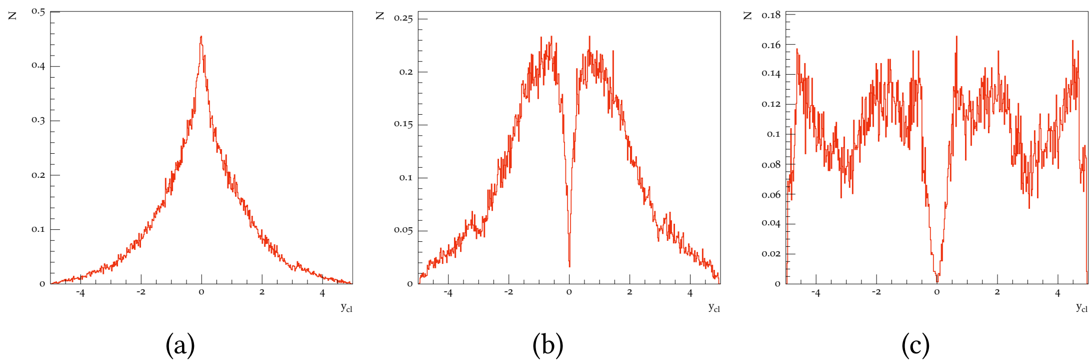

Figure 5.6: Rapidity distribution of final clusters relative to the momentum axis of the primary cluster constituents. P_{split} is varied from $P_{split} = 0.5$ shown in (a) to $P_{split} = 5.0$ shown in (c), whereas in (b) $P_{split} = 1.0$.

5.4.1 Results

Sampling y_1 and y_2 directly according to a power law can describe data for the mean charged multiplicity. As can be seen in Fig. 5.7a data lies within the band of possible parameter values. The same holds true for the scaled momentum x_p in Fig. 5.7b and for the thrust major M in Fig. 5.7d. In both cases data is only described by boundary values of P_{split} and the range of possible distributions is again several magnitudes wide in certain regions. For higher values of $1 - T$, shown in Fig. 5.7c, data is not described within the tested range of parameter values.
Following the conclusion of the other approaches it does not seem to be beneficial to tune this model to data since the distribution of the rapidity is unstable and not uniformly

distributed, shown in Fig. 5.6. This can also be seen in Fig. 5.7 illustrated by the width of the bands.
The mixed distribution of an exponential and a power law approach does not show any significant improvement compared to either of the two alternative approaches described before. There is no significant difference shown as the resulting distributions have the same characteristics as one of the two component distributions.

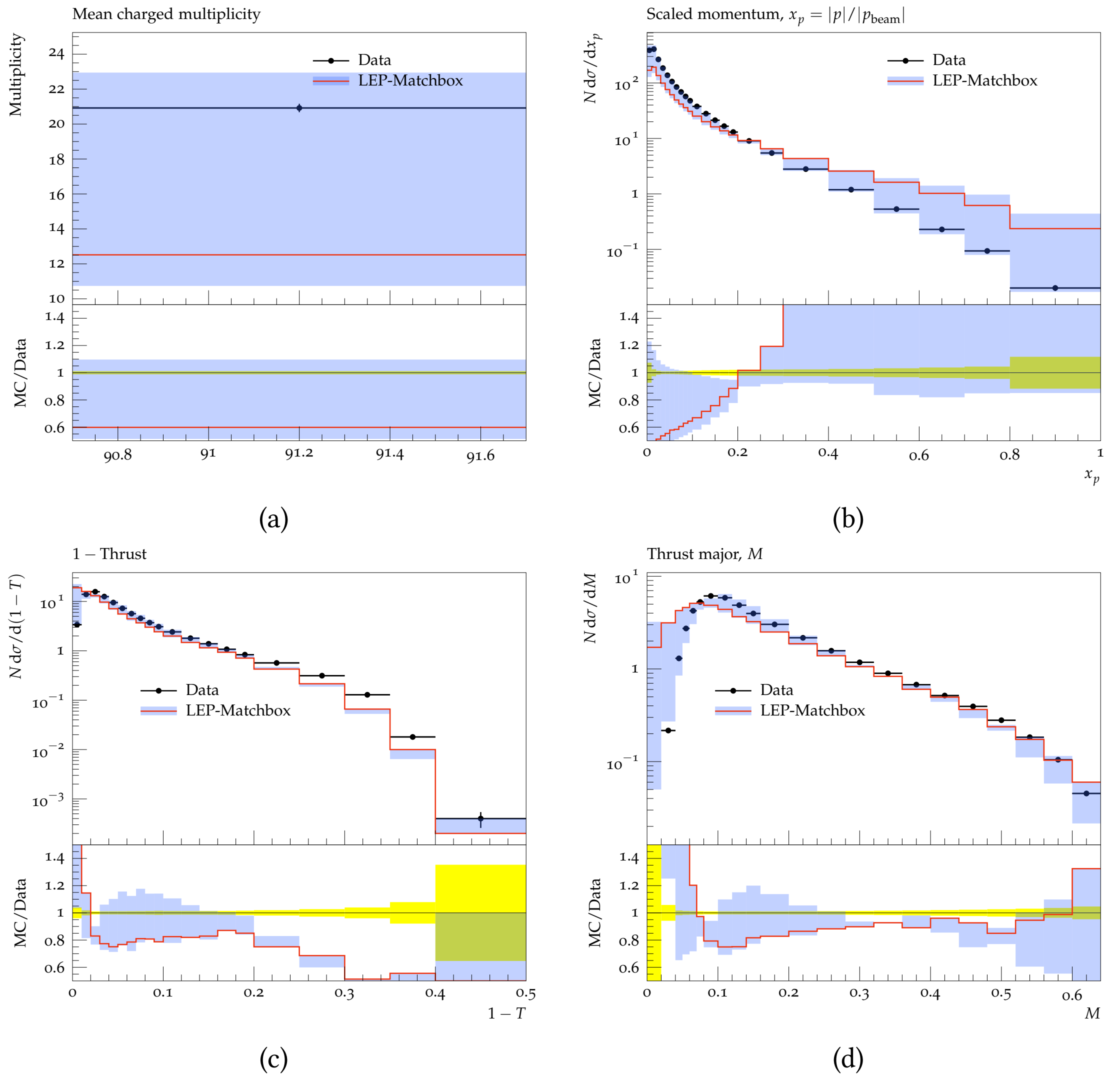

Figure 5.7: Possible regions of observables [31] sampling y_1 and y_2 according to power law. P_{split} is varied from $P_{split} = 0.3$ to $P_{split} = 9.0$. The red line indicates runs with $P_{split} = 3.0$.

5.5 Conclusion

The main idea in this chapter was to keep the sequential two body decay of clusters that undergo fission but try to distribute them more uniformly in rapidity relative to

the momentum direction of the primary cluster's constituents. This was done in several approaches by sampling the children clusters' rapidities instead of their masses. Firstly, to sample in rapidity, Δy, y^*, y_1 and y_2 had to be calculated and the boundaries on masses translated to boundaries on rapidity values. With this, different probability density functions for sampling rapidities were tested and compared to data observables.
For a power law approach some data was not described within the parameter range and therefore the approach was not further investigated. Sampling according to an exponential law is promising for a small range of parameter values but seems to be too unstable to tune. Overall it also proved difficult to maintain a stable distribution for the sequential rapidity sampling, which can be seen in Figs. 5.4 and 5.6. Over the course of this thesis only two of the many known probability distribution functions were used for the rapidity sampling. Therefore the approach to sequentially sample the cluster rapidities can not be completely ruled out as a possible improvement to the current hadronisation model. The rapidity sampling with a mixed distribution was only a small test for sampling approaches beyond the two mainly discussed distributions. For the following part of this thesis it was then decided to get rid of the sequential two body decay and not examine any other probability distributions. Instead of sequentially fissioning into two clusters the appropriate clusters fission directly into N children clusters. This will be discussed in detail in the following chapter. Beyond the scope of this work it would be interesting to see if other distributions prove to be more stable and are able to produce final clusters which are uniformly distributed in rapidity.

6 1 to N decay

A downside of sequential two body decays is that the distributions of the final clusters proved to be difficult to model. The direct decay of one or two particles (clusters) into N particles (clusters), shown in figure 6.1, makes the distributions easier to model. As a "2 to N decay" has been used to describe the physics of the underlying event (UE) a "1 to N decay" might also prove useful in the description of the hadronisation. With the release of Herwig 7.1 another "2 to N decay" is implemented as the default model for soft interactions in the UE again. There it improves the description of data significantly [30] and strengthens the assumption that such a model might also improve the hadronisation. A similar "2 to N decay" is used in the UA5-model [34] for an outdated description of the underlying event. It is still implemented in Herwig 7, but not used as the default model of the UE anymore. The basis of the UA5-model is an algorithm proposed by S. Jadach [35] which allows the calculation of the n-particle phase space with limited computational resources.
As part of this thesis a cluster fission into N clusters was implemented and tested. Therefore in the following section firstly the algorithm by Jadach is described after which the implementation of the UA5-model in Herwig 7 is outlined and differences to the implementation of a 1 to N decay in the hadronisation are shown. Conclusively resulting distributions and potential further investigations will be discussed.

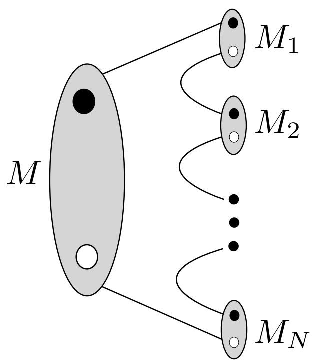

Figure 6.1: 1 to N decay.

6.1 UA5 Parametrisation of the Underlying Event

6.1.1 Jadach Algorithm

The main idea of the algorithm proposed by Jadach [35] is to transform a phase space integral for n particles that conserves energy and momentum into a form suitable for

Monte-Carlo integration,

$$\int_{\Omega} \prod_i \mathrm{d}\xi_i f(\xi_i) = \lim_{N\to\infty} \frac{1}{N} \sum_{I=1}^{N} \frac{1}{\rho_G(\xi_I)} f(\xi_I), \tag{6.1}$$

where the estimation on the right hand side converges to the true value of the desired integral on the left hand side in the limit of large numbers. $\rho_G(\xi_I)$ is the normalised probability distribution of a random number ξ_I.

6.1.1.1 Mathematical Background

Starting off with the phase space integral for n particles [35],

$$I_n = \int \prod_{i=1}^{n} \frac{\mathrm{d}^3 p}{2E_i} \delta^3\left(\sum_i^n p_i\right) \delta\left(w - \sum_{i=1}^{n} E_i\right) F(\mathbf{p}_1, \mathbf{p}_2, \dots, \mathbf{p}_n), \tag{6.2}$$

where $\mathbf{p}_i$ is the four momentum of particle i and w the total energy, the first step is to split the general four momentum into longitudinal momentum and transverse momentum relative to the direction of incoming particles. The transverse momentum is given by two components u_i and v_i,

$$\mathbf{p}_i = (E_i, p_i^L, p_i^T) = (E_i, p_i^L, u_i, v_i). \tag{6.3}$$

The phase space integral can then be rewritten as a product,

$$I_n = \int \prod_{i=1}^{n} \mathrm{d}u_i \mathrm{d}v_i \delta\left(\sum_{i=1}^{n} u_i\right) \delta\left(\sum_{i=1}^{n} v_i\right) \cdot L_n, \tag{6.4}$$

with L_n being the integral over the longitudinal momentum

$$L_n = \int \prod_{i=1}^{n} \frac{\mathrm{d}p_i^L}{2E_i} \delta\left(\sum_{i=1}^{n} p_i^L\right) \delta\left(w - \sum_{i=1}^{n} E_i\right) F. \tag{6.5}$$

In Eq. 6.4 the δ-distributions of u and v can be eliminated via change of variables,

$$\begin{aligned} u_i &= s_i + \lambda a_i, \\ \mathbf{a} &= \frac{1}{\sqrt{n}}(1, 1, \dots, 1), \\ \mathbf{s} \cdot \mathbf{a} &= 0. \end{aligned}$$

The integral over u_i can then be written as

$$\int \prod_{i=1}^{n} \mathrm{d}u_i \delta\left(\sum_{i=1}^{n} u_i\right) = \int \prod_{i=1}^{n-1} \mathrm{d}s_i \mathrm{d}\lambda \delta(\sqrt{n}\lambda) = \frac{1}{\sqrt{n}} \int \prod_{i=1}^{n-1} \mathrm{d}s_i, \tag{6.6}$$

where the δ-distribution completely disappeared and Eq. 6.1 can be used. For v it is possible to do the same variable change. This leads to an integral over the transverse momentum that is completely free of δ-distributions and according to Eq. 6.1 it can be written as

$$I_n = \lim_{N\to\infty} \frac{1}{N} \sum_{i=1}^{N} \frac{(\pi R)^{n-1}}{n} \exp\left(\frac{\sum \left(p_i^T\right)^2}{R}\right) \cdot L_n, \tag{6.7}$$

where R is a constant, dependent on the average transverse momentum p_T of all generated events. It is given by

$$R = \frac{4}{\pi} p_T^2 \left(1 + \frac{1}{n-1}\right). \tag{6.8}$$

To reach Eq. 6.7 it is also used that s_i is randomly generated with the probability distribution

$$\rho_G(\mathbf{s}) = (\pi R)^{-\frac{1}{2}(n-1)} \exp(-\mathbf{s}^2/R). \tag{6.9}$$

With the transverse phase space integral rewritten to a form suitable for Monte Carlo integration the next task is to rewrite the longitudinal phase space integral. According to [35] it is best to introduce the rapidity variable as it simplifies the phase space element and gets rid of any factors in the phase space element that could result in singularities if energy increases. In terms of rapidity the longitudinal phase space integral is

$$\begin{aligned} L_n &= 2^{1-n} \int \prod_{i=1}^{n} \mathrm{d}y_i \delta\left(w - \sum_{i=1}^{n} m_i^T \exp(y_i)\right) \delta\left(w - \sum_{i=1}^{n} m_i^T \exp(-y_i)\right) F \\ &= w 2^{1-n} \int \prod_{i=1}^{n} \mathrm{d}y_i \delta\left(w^2 - \left(\sum_{i=1}^{n} m_i^T \exp(y_i)\right)\left(\sum_{i=1}^{n} m_i^T \exp(-y_i)\right)\right) \delta\left(w - \sum_{i=1}^{n} m_i^T \exp(y_i)\right) F, \end{aligned} \tag{6.10}$$

where the transverse mass is introduced as

$$m_i^T = \sqrt{m_i^2 + p_i^{T2}}. \tag{6.11}$$

Similar to the transverse part the following variable transformation is performed

$$y_i = Z + Y\xi_i, \tag{6.12}$$

with

$$\begin{aligned} &\xi_1 \equiv 0, && \xi_n \equiv 1, \\ &0 \le \xi_i \le 1, && i = 2, 3, \ldots, n-1. \end{aligned} \tag{6.13}$$

Where ξ_i is called the prerapidity. The longitudinal phase space integral then takes the form

$$\begin{aligned} L_n = w 2^{1-n} \int \mathrm{d}Z \mathrm{d}Y \prod_{i=2}^{n-1} \mathrm{d}\xi_i Y^{n-2} \delta\left(w^2 - \left(\sum m_i^T \exp(\xi_i Y)\right)\left(\sum m_i^T \exp(-\xi_i Y)\right)\right) \\ \delta\left(w - e^Z \left(\sum m_i^T \exp(\xi_i Y)\right)\right) F, \end{aligned} \tag{6.14}$$

with which the integration over Y and Z can be performed and the δ-distributions disappear. This then leads to

$$L_n = 2^{1-n} \int \prod_{i=2}^{n-1} \mathrm{d}\xi_i \frac{Y^{n-2}}{Dw^2} F, \tag{6.15}$$

and Eq. 6.1 can then be used, resulting in

$$L_n = \lim_{N\to\infty} \frac{1}{N} \sum_{I=1}^{N} \frac{n(n-1)Y^{n-2}}{2^{n-1}w^2 D} F(\xi_I), \tag{6.16}$$

where

$$D = \left| \frac{\partial}{\partial Y} \ln \left(\left(\sum_i m_i^T \exp(\xi_i Y) \right) \left(\sum_i m_i^T \exp(-\xi_i Y) \right) \right) \right|. \tag{6.17}$$

Now that the whole phase space integral can be written in a way suitable for Monte Carlo integration an algorithm can be applied to calculate the n-particle phase space integral. This is described in the next section.

6.2 Implementation

In this work the algorithm proposed by Jadach was implemented in to the hadronisation following it's implementation in the UA5 simulation program [34]. This section will therefore describe how the Jadach Algorithm is implemented in the UA5 model for the underlying event and point out differences to the implementation in the hadronisation where they occur.

6.2.1 UA5-model

The first step is to determine the number of charged particles n_{ch} by drawing it from a negative binomial distribution,

$$P(n;\langle n\rangle,k) = \binom{n+k-1}{k-1} \left(\frac{\frac{\langle n\rangle}{k}}{1+\frac{\langle n\rangle}{k}} \right)^n \frac{1}{\left(1+\frac{\langle n\rangle}{k}\right)^k}. \tag{6.18}$$

$\langle n\rangle$ is the average number, k is a shape parameter and both are taken from fits to data. After the number of charged particles is determined, the composition of the produced particles has to be generated. This is in principle done by cluster formation and decay. Two leading clusters always consist of a nucleon, a Δ or their antiparticles. The other clusters, whose compositions are determined by Poisson distributions, contain a nucleon pair, a baryon pair (except for π) or at least one π. At each step the number of particle types is drawn from these Poisson distributions which depend on measured ratios of different particle types.

These newly produced clusters are then given momenta. Following the Jadach Algorithm this is done in two steps, first the transverse momentum then the longitudinal momentum is generated. The transverse momenta are generated following an exponential distribution

$$\frac{dN}{dp_T^2} \propto e^{-b \cdot p_T}, \tag{6.19}$$

where their azimuthal directions are uniformly drawn between 0 and 2π. The momenta in the plane perpendicular to the beam axis are conserved, therefore two independent linear transformations are performed for each of the two transverse momentum axes

$$p_i^{new} = p_i^{old} - \frac{\left(\sum_{\text{all clusters in event}} p_i^{old}\right)}{N} \qquad i = u, v. \tag{6.20}$$

As described in Eq. 6.12 et seq. at first prerapidities are generated following a certain probability distribution. In this case a "flat central part with gaussian wings" ([34], p.455), as seen in figure 6.2, was found to give good agreement with data. The leading clusters are

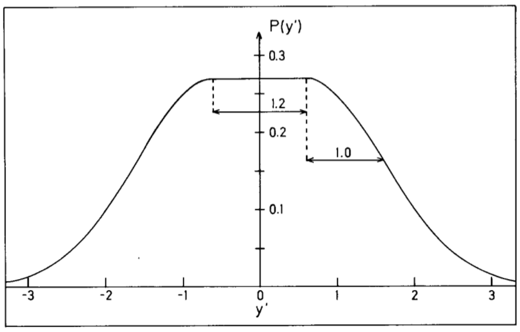

Figure 6.2: Probability distribution of prerapidity [34].

assigned to the highest and the lowest prerapidities whereas the remaining prerapidities are randomly distributed among the other clusters. With the generated prerapidities the rapidities are calculated using Eq. 6.12. Z is determined from p_L conservation and Y from energy conservation. Finally with the transverse mass m_T the longitudinal momentum p_L is calculated.

6.2.2 Implementation in the hadronisation

In contrast to the UA5-model there are no leading clusters in the description of solely the hadronisation as there are no beam remnants considered in this thesis. For each cluster that fulfils Eq. 4.1 the number N of clusters it fissions to is determined by an evolution of rapidity y from y_{max} to 0. Contrary to Eq. 6.18, where $\langle n \rangle$ and k are fitted to data at certain energies, an evolution for N is variable and can be used for all energies. One main goal of an evolution in rapidity is to have a constant mean number of clusters $\langle n \rangle$ per rapidity interval Δy,

$$\frac{\langle n \rangle}{\Delta y} \approx \text{const.} \tag{6.21}$$

To get y_{max} the rapidity of the two cluster constituents is calculated in the centre of mass frame of the fissioning cluster according to

$$y_{max} = \log\left(\frac{\sqrt{m_{q_1}^2 + p^{*2}} + p^*}{m_{q_1}}\right), \tag{6.22}$$

with the momentum p^* given by

$$p^* = \frac{\sqrt{M^4 + m_{q_1}^4 + m_{q_2}^4 - 2m_{q_1}^2 m_{q_2}^2 - 2M^2 m_{q_1}^2 - 2M^2 m_{q_2}^2}}{2M}. \tag{6.23}$$

Starting from y_{max} the probability to split a cluster is given by an exponential probability distribution, comparable to nuclear decay. The new starting rapidity is then given by the difference of the initial rapidity and the calculated rapidity segment Δy, see Eq. 6.24.

$$\begin{aligned} y_0 &= y_{max} \\ \Delta y &= \alpha e^{-\alpha x} \\ y_{i+1} &= y_i - \Delta y \end{aligned} \tag{6.24}$$

After the number of clusters is determined, generation of the phase space is mostly following the implementation of the UA5-model, except for the probability distribution of the transverse momentum. Instead of an exponential distribution, like in Eq. 6.9, a normal distribution

$$f(\mu, \sigma) = \frac{1}{\sqrt{2\pi\sigma^2}} e^{-\frac{(x-\mu)^2}{2\sigma^2}}, \tag{6.25}$$

is chosen to have direct influence on the mean transverse momentum of the produced clusters. μ and σ are then two additional parameters introduced with the mean transverse momentum μ and the variance σ of the transverse momentum distribution. The distribution can also be parametrised according to

$$\frac{\mathrm{d}\sigma}{\mathrm{d}p_\perp^2} \sim e^{-\left(\frac{p_\perp}{2p_\perp^0}\right)^2}, \tag{6.26}$$

where $p_\perp^0$ is the mean transverse momentum and tuning is therefore performed to a more physical parameter. For every newly produced cluster a quark antiquark or diquark antidiquark pair is produced from the vacuum and distributed among the clusters illustrated in Fig. 6.3. Their flavour is randomly chosen according to weights defined in the parameters $PwtUDquark$, $PwtCquark$, $PwtSquark$, $PwtDiquark$. An overview of all parameters used in this model is given in Table 6.1.

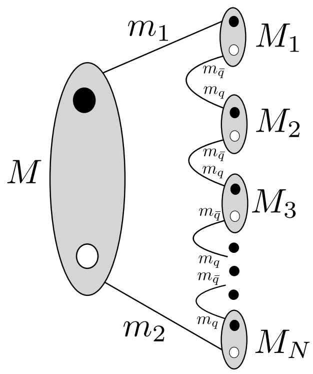

Figure 6.3: Choosing flavour of newly produced clusters.

Table 6.1: Description of parameters in the default cluster fission model.

Parameter	Description
EvolutionMean	Sets the α value in Eq. 6.24
*EvolutionM*1	Parameter for the random mass of a newly produced cluster in GeV
*EvolutionM*2	Parameter for the random mass of a newly produced cluster in GeV^{-1}
PTslope	Deviation of gaussian p_T sampling.
PTmean	Mean value of gaussian p_T sampling.
PwtUDquark	Weight for ud-flavoured quarks.
PwtCquark	Weight for c-flavoured quarks.
PwtSquark	Weight for s-flavoured quarks.
PwtDiquark	Weight for Diquarks.

6.3 Toy model

Before the 1 to N decay is implemented in Herwig 7 the algorithm is tested in a small Python script to determine its properties. This section will give a brief overview of the properties of this toy model.

The mean number of produced clusters, shown in Fig. 6.4a, is linearly dependent on the logarithm of the centre of mass energy. As a result of this linear dependence the mass distribution of final clusters should be independent of the centre of mass energy, which can be seen in Fig. 6.4b. Since one goal of an alternative approach to cluster fission is a uniform distribution in rapidities of final clusters, it is interesting to see the rapidity distributions of the toy model. In Figs. 6.4c ($\alpha = 1.0$) and 6.4d ($\alpha = 5.0$) the rapidity distributions are shown relative to a fixed z-axis. The rapidities are not just uniformly distributed but also seem to be stable when varying α or the centre of mass energy. For the sake of completeness the mass distribution and the rapidity distribution are shown in Figs. 6.4e and 6.4f. Both are in the range expected from the previous discussion.

The toy model shows that the algorithm from the UA5-model for 1 to N decays is the desired approach. In the following section the algorithm will be implemented in the hadronisation of Herwig 7 and its parameters determined to best describe data.

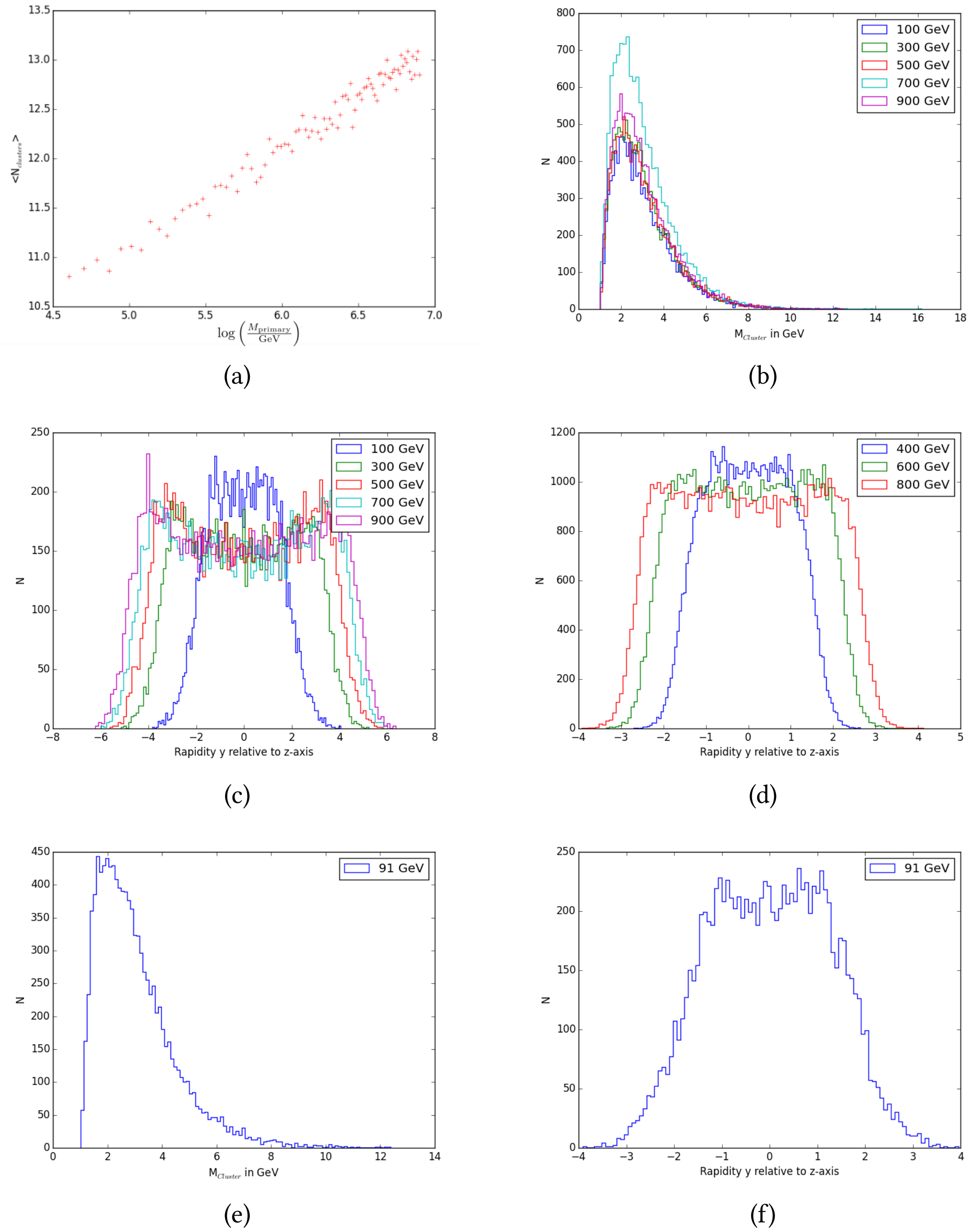

Figure 6.4: Distributions from the toy model implementation. Figs. (a)-(c) show distributions for $\alpha = 1.0$ (see Eq. 6.24) at different centre of mass energies. In Fig. (d) the rapidity distributions of $\alpha = 5.0$ are shown for different centre of mass energies. Figs. (e) and (f) show the distributions for fixed α at a centre of mass energy of 91.2 GeV.

6.4 Tuning

Since the new approach introduces nine new parameters, their values have to be constrained. This is done by using experimental data and is called generator tuning. The framework used for tuning is the PROFESSOR tuning system [36], the analyses used are provided by Rivet [37] and are listed in Appendix A.1. In all tuning runs the process considered is $e^+e^- \to jj$ at the centre of mass energy of 91.2 GeV. The parameters described in Table 6.1 plus the parton shower cut-off $pTmin$ are tuned to multiplicities, shape variables and other observables for two different ranges of p_T, see Range 1 and Range 2 in Table 6.2. All of the used observables and their weights are listed in Tables A.1-A.18. In Fig. 6.5 it can be seen that the restriction of $EvolutionMean$ to a smaller range is in agreement with charged multiplicity so that simulation runs are able to describe data. According to [36] the minimum number of runs N for a given number of parameters P is

$$N_n^{(P)} = 1 + \sum_{i=1}^{n} \frac{1}{i!} \prod_{j=0}^{i-1} (P + j), \tag{6.27}$$

where n is the order of the polynomial used to fit. In this case the number of parameters to tune is $P = 10$, since $pTmin$, the cut-off value of the parton shower, has significant impact on the hadronisation and therefore is also tuned. With a higher parton shower cut-off, bigger clusters, subsequently more final clusters and higher hadron multiplicities are to be expected. The inverse argument applies for smaller values of $pTmin$. For ten parameters the minimum number of runs is $N_3^{(10)} = 286$ for a polynomial of order $n = 3$. Since [36] suggests oversampling by a factor of at least 2, the minimum number of runs is $2N_3^{(10)} = 572$. In this thesis the number of runs in both cases is between $N = 700$ and $N = 800$ with 1000000 events for each set of parameter ranges. The exact number of successful runs is not clear in advance because of a yet unknown bug which causes some (less than 100) of the 800 initial runs to not finish at all, these runs can not be used further.

Table 6.2: Parameter ranges for tuning.

Parameter	**Range 1**	Tune 1		**Range 2**	Tune 2	
		mult.	gen.		mult.	gen.
$EvolutionMean$	**1.15-1.17**	1.169942	1.169942	**1.15-1.17**	1.168298	1.166815
$EvolutionM1$	**0.1-5.0**	0.872854	0.875266	**0.1-5.0**	0.741735	0.646280
$EvolutionM2$	**50-600**	599.258800	599.25880	**50-600**	339.451746	68.946236
$PTslope$	**1.0-10.0**	1.004623	1.004623	**1.0-10.0**	1.001118	9.120575
$PTmean$	**1.0-10.0**	1.013010	1.013010	**1.0-10.0**	1.010316	3.504758
$PwtUDquark$	**0.0-10.0**	5.913285	5.783869	**0.0-10.0**	9.996982	0.224378
$PwTCquark$	**0.0-10.0**	0.005470	0.005470	**0.0-10.0**	1.220182	0.272114
$PwTSquark$	**0.0-10.0**	7.806019	7.642248	**0.0-10.0**	0.028829	9.712178
$PwTDiquark$	**0.0-10.0**	0.028466	0.028466	**0.0-10.0**	9.991533	5.837031
$pTmin$	**4.0-5.0**	4.000184	4.000184	**0.5-5.0**	4.991475	0.601294

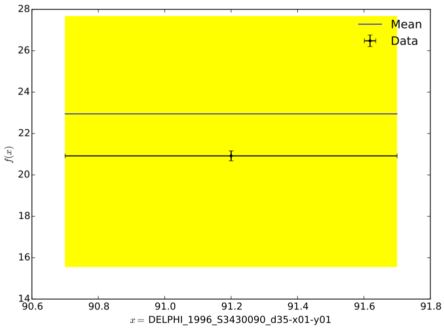

(a)

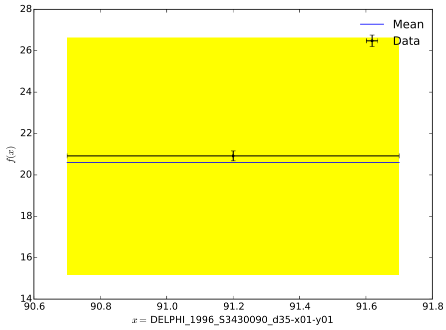

(b)

Figure 6.5: Possible mean charged multiplicity values for 1 to N decay. In (a) Range 1 ($pTmin$ = 4.0-5.0) is shown and in (b) Range 2 ($pTmin$ = 0.5-5.0) is shown.

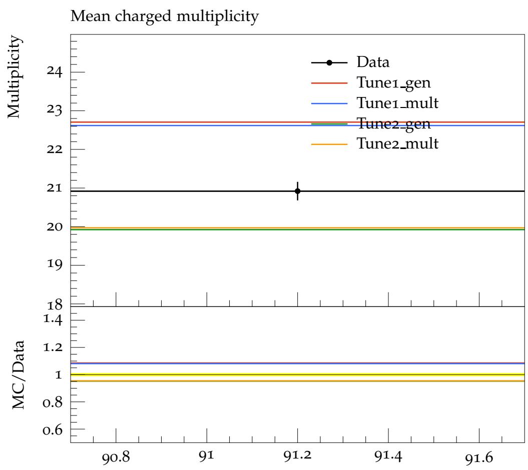

(a)

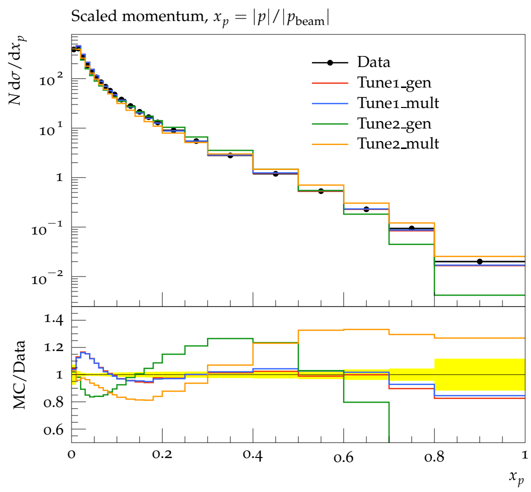

(b)

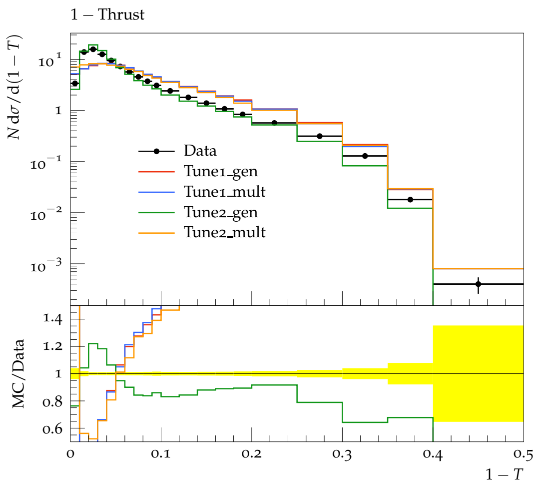

(c)

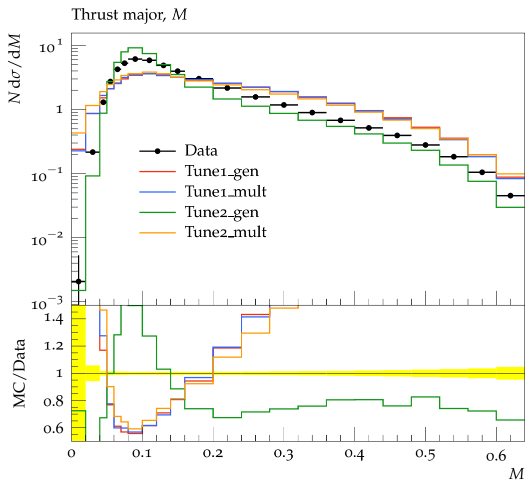

(d)

Figure 6.6: Runs with different tunes of parameters for the 1 to N decay.

6.5 Results

For both tuning runs the parameters are first tuned to only multiplicities (labelled as "mult.") and then tuned to a more general selection of observables (labelled as "gen."). The resulting parameter values for the four tunes are listed in Table 6.2. There is a noticeable influence that $pTmin$ seems to make on the overall shape of the hadronisation. Both tuning runs for Tune 1 in Table 6.2, where $pTmin$ only varies in a range of 1 GeV, result in very similar parameter values. Unlike Tune 1, the results of the tuning runs from Tune 2, where $pTmin$ varies in the range of 4.5 GeV, differ noticeably.
To see how well the simulation performs with the tuned parameters, simulation runs with these tuned parameter values are carried out. The results of runs with the four tunes are shown in Fig. 6.6. Again, the first observable to look at is the mean charged multiplicity, shown in Fig. 6.6a. Although the tunes were performed specifically to multiplicity distributions, with the highest weight on the mean charged multiplicity, none of the tuned parameter sets describe the mean charged multiplicity within 5% deviation. Tune 1 produces too many charged particles and Tune 2 produces too few charged particles. Despite the tuned values being so different in Range 2, the mean charged multiplicity is almost identical. This can be explained by looking at the value for $pTmin$. For Tune 2 (mult.), where $pTmin = 4.991475$ GeV, fewer initial clusters are produced than for Tune 2 (gen.), where $pTmin = 0.601294$ GeV, because the shower stops at higher energies. Consequently, these clusters have higher masses and fission into more clusters. In the second case, $pTmin = 0.601294$ GeV, there is a greater number of initial clusters and more of these clusters have masses below the fission threshold so that they do not fission into additional clusters. This means that the shape of considered distributions is mostly defined by the hadronisation for $pTmin = 4.991475$ GeV and by the parton shower for $pTmin = 0.601294$ GeV.
The scaled momentum x_p, shown in Fig. 6.6b, is not well described by any of the tunes. At best it is described within 20% deviation by the tunes from Range 1. Tunes from Range 2 in parts differ by a deviation of more than 20%, Tune 2 (gen.) differs for high x_p by even more than 40%. Considering that this range of x_p is sensitive to the hadronisation it is plausible that in Tune 2 (gen.) the hadronisation model does not have enough impact on the momenta of the clusters as they are, in most cases, already determined by the parton shower.
In Fig. 6.6c the $1-T$ distribution is shown. For both Tune 1 and Tune 2 (mult.) data is poorly described with deviations between data and simulation runs of more than 40%. Tune 2 (gen.) on the other hand improves the description noticeably and is for $1 - T < 0.3$ within 20% deviation. However, in the region $1 - T \to 0.5$ Tune 2 (gen.) does not describe data very well as the simulation deviates by more than 40% for $1 - T > 0.4$. The improvement of Tune 2 (gen.) compared to Tune 1 and Tune 2 (mult.) is also visible in the thrust major distribution, shown in Fig. 6.6d. For all of the latter three tunes data is poorly described with deviations of more than 40% compared to data. Tune 2 (gen.), although an improvement, has for $M > 0.2$ around 20% deviation and increases to more than 40% for $M < 0.2$. Both thrust variables are, like the scaled momentum, poorly described by the tunes where hadronisation plays a bigger role (Tune 1 and Tune 2 (mult.)). Tune 2

(gen.) consequently describes data better in regions where the parton shower is of more importance than in regions sensitive to hadronisation.

6.6 Conclusion

In this chapter a new approach to cluster fission was implemented and examined. The main idea is that clusters, which fulfil the inequality Eq. 4.1, fission into N clusters instead of two. This makes distributions of final clusters easier to model, for example rapidity distributions. A very similar approach was already used for the description of the UE by the UA5-model and therefore the implementation in the hadronisation follows the UA5-model closely.
A first analysis of this approach in a small Python script, which solely simulates the 1 to N decay, shows promising results. Rapidities of the final clusters are uniformly distributed, which is commonly witnessed in soft physics and might therefore be an improvement for the hadronisation. The number of produced clusters depends linearly on the logarithm of the centre of mass energy and the mass distribution is independent of the centre of mass energy.
After this test the 1 to N decay was implemented in the hadronisation model of Herwig 7. As an alternative to the current cluster fission in Herwig 7 it can be used in the same place in the event generation without restrictions on surrounding classes. The new fission model introduces nine parameters which so far have not been tuned to values where they describe data best. In addition to the nine parameters introduced by the 1 to N decay, the minimum cut-off scale, p^T_{min}, is tuned as well since it has significant impact on hadronisation properties. At a centre of mass energy of 91.2 GeV for the process $e^+e^- \rightarrow jj$ and two different parameter ranges, two tuning runs are performed for each parameter range. Firstly the parameters are tuned to solely multiplicity distributions and secondly additional observables are taken into account. Although the mean charged multiplicity can be described by the parameter values considered, all tuned parameter values do not describe mean charged multiplicity data very well. For the other observables, e.g. x_p, $1-T$ and M, none of the tuning runs so far produces parameter values that result in better simulations than the current hadronisation model.
Despite the negative results so far the "1 to N decay"-approach remains interesting. In all the observable distributions considered, all regions can be theoretically described by the model so it cannot be disqualified by a first look at the observable distributions. It rather seems that the introduced parameter space of ten parameters is so complex that the tuning runs performed in this thesis tune in the wrong region of the parameter space and should be constrained to a smaller parameter range. Additionally, the newly introduced parameters should be tuned to parameters of the colour reconnection, as it has significant impact on cluster properties. The colour reconnection has not been taken into account for the tunes in this thesis.
Another point that has to be taken into account is that the toy model was mostly used for centre of mass energies higher than 91.2 GeV. For these energies the "1 to N decay"-algorithm does not seem to have any problems with generating the expected number of clusters. In energy regions below 91.2 GeV it turns out to be more complex to maintain the

linear dependence of the number of produced clusters on the logarithm of the centre of mass energy. For the process considered in this thesis, 91.2 GeV is the highest mass a cluster is able to have and with the parton shower turned on it is more likely that initial clusters have masses far below 91.2 GeV. Therefore, it is of greater interest to fully understand the behaviour of the 1 to N decay, especially in regions of low centre of mass energies. It might turn out that the 1 to N model is a too general description to be used in event generations with parton showers and is only useful for decays with high centre of mass energies.

Another question that emerged recently, which is worth looking into in the future, concerns the ordering of the cluster constituents in rapidity. Contrary to the 2 to N model in the UE, where the gluons are ordered in rapidity, the 1 to N model of the hadronisation orders the clusters in rapidity and not their constituents. At first sight this does not make sure that the constituents are strictly ordered in rapidity as there might be an overlap between constituents of different clusters.

7 Summary and Outlook

In order to improve the description of LEP-observables the aim of the present thesis is to discuss several alternative approaches to the hadronisation model used in Herwig 7 and review if they are an improvement.
For this purpose properties of the current hadronisation of Herwig 7 are examined and it is seen that shortcomings in description of data are in observables sensitive to hadronisation. In a first approach the general structure of the algorithm is kept and only the determination of the children clusters' properties is changed. This means that clusters still fission into two children clusters and the fission is done recursively until clusters' masses are below a certain threshold. Instead of sampling the children cluster masses, their rapidities are sampled randomly. Sampling both rapidities independently according to a power law, analogously to the currently implemented mass sampling, proves to be no improvement to the current sampling. Rapidity distributions are unstable and data within the examined parameter range is not sufficiently well described.
For additional approaches the "relative rapidity" Δy and the "centre of mass" rapidity y^* are introduced, defined in Eq. 5.2. Δy and y^* are then firstly sampled according to a power law and secondly according to an exponential law.
The power law approach for Δy and y^* is not able to sufficiently describe the mean charged multiplicity, an observable very well described by the current hadronisation model, for the examined parameter values. Other observables, such as the thrust or the scaled momentum, are not well described by runs with the power law sampling. Another approach is therefore examined, sampling Δy and y^* according to an exponential law. With an exponential sampling data is described by the simulation in general within the used parameter range. For certain parameter values, that describe data best in this model, the rapidities of final clusters are also uniformly distributed. This is a desired distribution as soft physics seems to be commonly described by uniform distributions in rapidity. Tuning this model however seems to be unreasonable as the distributions are very unstable when changing the two introduced parameters by small values.
In the last approach considered, the fissioning cluster does not decay into N clusters by sequential two body decays but fissions directly into N clusters uniformly distributed in rapidity. The occurring n-dimensional phase space integral is solved according to an algorithm which samples rapidities uniformly. The implementation of a 1 to N cluster fission follows the UA5-model, used as an outdated description of the UE, closely but with some differences. The main difference is in the determination of the number of children clusters. The UA5-model determines the number of produced particles by sampling from a negative binomial distribution. In this thesis it is done as an evolution of rapidity from $y_{\max}$ to 0 so that the number of produced clusters is sensible for all energies. In a first test this approach seems to give the desired properties of the final clusters and was therefore implemented in Herwig 7. The newly introduced parameters have to be tuned to data

from scratch since there are no comparable parameter values. All tunes performed during the work on this thesis result in simulation runs that are no improvement to simulation runs with the current hadronisation model. But for several reasons the 1 to N decay still seems to be an approach that is able to improve the hadronisation of Herwig 7. First of all, every distribution considered in this work can be described by the "1 to N decay"-model and changes in parameters have a significant impact on the shapes of distributions. Secondly, the parameter space introduced is quite complex with at least 10 parameters to tune. Therefore, the tunes performed in this thesis might be in the wrong region of the parameter space but due to lack of time further regions are not considered here. Thirdly, the 1 to N decay proved to be more difficult than expected for lower centre of mass energies, especially below 91.2 GeV. Here the linear dependence of the number of clusters on the logarithm of the centre of mass energy is not ensured. It might prove that the "1 to N decay"-model is a too general description for low centre of mass energies.
Another open question is the ordering of cluster constituents in rapidity. So far only the clusters are ordered in rapidity but the cluster constituents might not be due to overlapping clusters.
For future work on hadronisation models it still remains interesting to take a closer look at the 1 to N decay. Over the course of this thesis the model could not be ruled out as an improvement to the current hadronisation model of Herwig 7. Moreover several aforementioned aspects of the 1 to N decay imply that it still might be a suitable model to describe hadronisation in event generators. Additionally, the rapidity sampling in sequential two body decays is not completely ruled out and might prove to be a reasonable alternative to the mass sampling currently used in Herwig 7. In this thesis only two distributions for sampling rapidities were discussed, an exponential law and a power law, as the focus of this work was then shifted to the 1 to N decay. In future it is therefore interesting to look at other probability distributions for rapidity sampling.
Finally it is interesting to discuss hadronisation in the context of the LHC. With higher centre of mass energies than LEP and therefore larger clusters the impact of an alternative cluster fission approach is expected to be more severe.

Bibliography

[1] Johannes Bellm et al. “Herwig 7.0/Herwig++ 3.0 release note”. In: *Eur. Phys. J.* C76.4 (2016), p. 196. DOI: 10.1140/epjc/s10052-016-4018-8. arXiv: 1512.01178 [hep-ph].

[2] Richard D. Field and Stephen Wolfram. “A QCD model for e+e- annihilation”. In: *Nuclear Physics B* 213.1 (1983), pp. 65 –84. ISSN: 0550-3213. DOI: https://doi.org/10.1016/0550-3213(83)90175-X. URL: http://www.sciencedirect.com/science/article/pii/055032138390175X.

[3] R. Keith Ellis, James Stirling, and B. R. Webber. *QCD and collider physics*. 1. paperback ed. Cambridge monographs on particle physics, nuclear physics, and cosmology ; 8. Includes index. Cambridge: Cambridge Univ. Press, 2003. ISBN: 0-521-58189-3; 0-521-54589-7.

[4] Lewis H. Ryder. *Quantum field theory*. 2. ed. Cambridge: Cambridge University Press, 1996. ISBN: 0-521-47242-3; 0-521-47814-6; 978-0-521-47814-4.

[5] Michael Edward Peskin. *An introduction to quantum field theory*. Ed. by Daniel V. Schroeder. Student economy edition. The advanced book program. [Boulder]: Westview Press, a member of the Perseus Books Group, [2016]. ISBN: 0-8133-5019-0; 978-0-8133-5019-6.

[6] William A. Bardeen et al. “Deep-inelastic scattering beyond the leading order in asymptotically free gauge theories”. In: *Phys. Rev. D* 18 (11 1978), pp. 3998–4017. DOI: 10.1103/PhysRevD.18.3998. URL: https://link.aps.org/doi/10.1103/PhysRevD.18.3998.

[7] C. Patrignani et al. “Review of Particle Physics”. In: *Chin. Phys.* C40.10 (2016), p. 100001. DOI: 10.1088/1674-1137/40/10/100001.

[8] M. Bahr et al. “Herwig++ Physics and Manual”. In: *Eur. Phys. J.* C58 (2008), pp. 639–707. DOI: 10.1140/epjc/s10052-008-0798-9. arXiv: 0803.0883 [hep-ph].

[9] Torbjorn Sjostrand, Stephen Mrenna, and Peter Z. Skands. “PYTHIA 6.4 Physics and Manual”. In: *JHEP* 05 (2006), p. 026. DOI: 10.1088/1126-6708/2006/05/026. arXiv: hep-ph/0603175 [hep-ph].

[10] T. Gleisberg et al. “Event generation with SHERPA 1.1”. In: *JHEP* 02 (2009), p. 007. DOI: 10.1088/1126-6708/2009/02/007. arXiv: 0811.4622 [hep-ph].

[11] Andy Buckley et al. “LHAPDF6: parton density access in the LHC precision era”. In: *Eur. Phys. J.* C75 (2015), p. 132. DOI: 10.1140/epjc/s10052-015-3318-8. arXiv: 1412.7420 [hep-ph].

[12] J. Alwall et al. "The automated computation of tree-level and next-to-leading order differential cross sections, and their matching to parton shower simulations". In: *Journal of High Energy Physics* 2014.7 (2014), p. 79. ISSN: 1029-8479. DOI: 10.1007/JHEP07(2014)079. URL: https://doi.org/10.1007/JHEP07(2014)079.

[13] J. Baglio et al. "Release Note - VBFNLO 2.7.0". In: (2014). arXiv: 1404.3940 [hep-ph].

[14] K. Arnold et al. "VBFNLO: A Parton level Monte Carlo for processes with electroweak bosons". In: *Comput. Phys. Commun.* 180 (2009), pp. 1661–1670. DOI: 10.1016/j.cpc.2009.03.006. arXiv: 0811.4559 [hep-ph].

[15] J. Baglio et al. "VBFNLO: A Parton Level Monte Carlo for Processes with Electroweak Bosons – Manual for Version 2.7.0". In: (2011). arXiv: 1107.4038 [hep-ph].

[16] Andy Buckley et al. "General-purpose event generators for LHC physics". In: *Phys. Rept.* 504 (2011), pp. 145–233. DOI: 10.1016/j.physrep.2011.03.005. arXiv: 1101.2599 [hep-ph].

[17] Stefan Gieseke, P. Stephens, and Bryan Webber. "New formalism for QCD parton showers". In: *JHEP* 12 (2003), p. 045. DOI: 10.1088/1126-6708/2003/12/045. arXiv: hep-ph/0310083 [hep-ph].

[18] Simon Platzer and Stefan Gieseke. "Coherent Parton Showers with Local Recoils". In: *JHEP* 01 (2011), p. 024. DOI: 10.1007/JHEP01(2011)024. arXiv: 0909.5593 [hep-ph].

[19] Simon Platzer and Stefan Gieseke. "Dipole Showers and Automated NLO Matching in Herwig++". In: *Eur. Phys. J.* C72 (2012), p. 2187. DOI: 10.1140/epjc/s10052-012-2187-7. arXiv: 1109.6256 [hep-ph].

[20] Günther Dissertori, Ian G. Knowles, and Michael Schmelling. *Quantum chromodynamics : high energy experiments and theory.* 1. publ. International series of monographs on physics ; 115. fälschl. als Bd. 112 bezeichnet; : £60.00 : Formerly CIP. Oxford [u.a.]: Clarendon Press, 2003. ISBN: 0-19-850572-8.

[21] S. Catani and M. H. Seymour. "A General algorithm for calculating jet cross-sections in NLO QCD". In: *Nucl. Phys.* B485 (1997). [Erratum: Nucl. Phys.B510,503(1998)], pp. 291–419. DOI: 10.1016/S0550-3213(96)00589-5,10.1016/S0550-3213(98)81022-5. arXiv: hep-ph/9605323 [hep-ph].

[22] B. Andersson et al. "Parton fragmentation and string dynamics". In: *Physics Reports* 97.2 (1983), pp. 31 –145. ISSN: 0370-1573. DOI: http://dx.doi.org/10.1016/0370-1573(83)90080-7. URL: http://www.sciencedirect.com/science/article/pii/0370157383900807.

[23] D. Amati and G. Veneziano. "Preconfinement as a property of perturbative QCD". In: *Physics Letters B* 83.1 (1979), pp. 87 –92. ISSN: 0370-2693. DOI: https://doi.org/10.1016/0370-2693(79)90896-7. URL: http://www.sciencedirect.com/science/article/pii/0370269379908967.

[24] G. Marchesini, L. Trentadue, and G. Veneziano. "Space-time description of colour screening via jet calculus techniques". In: *Nuclear Physics B* 181.2 (1981), pp. 335 –346. ISSN: 0550-3213. DOI: https://doi.org/10.1016/0550-3213(81)90357-6. URL: http://www.sciencedirect.com/science/article/pii/0550321381903576.

[25] Loyal Durand and Hong Pi. "High-energy nucleon-nucleus scattering and cosmic-ray cross sections". In: *Phys. Rev. D* 38 (1 1988), pp. 78–84. DOI: 10.1103/PhysRevD.38.78. URL: https://link.aps.org/doi/10.1103/PhysRevD.38.78.

[26] I. Borozan and M. H. Seymour. "An Eikonal model for multiparticle production in hadron hadron interactions". In: *JHEP* 09 (2002), p. 015. DOI: 10.1088/1126-6708/2002/09/015. arXiv: hep-ph/0207283 [hep-ph].

[27] Loyal Durand and Hong Pi. "Semihard QCD and high-energy pp and $\overline{p}p$ scattering". In: *Phys. Rev. D* 40 (5 1989), pp. 1436–1445. DOI: 10.1103/PhysRevD.40.1436. URL: https://link.aps.org/doi/10.1103/PhysRevD.40.1436.

[28] Manuel Bahr, Jonathan M. Butterworth, and Michael H. Seymour. "The Underlying Event and the Total Cross Section from Tevatron to the LHC". In: *JHEP* 01 (2009), p. 065. DOI: 10.1088/1126-6708/2009/01/065. arXiv: 0806.2949 [hep-ph].

[29] Johannes Bellm et al. "Herwig 7.1 Release Note". In: (2017). arXiv: 1705.06919 [hep-ph].

[30] Stefan Gieseke, Frashër Loshaj, and Patrick Kirchgaeßer. "Soft and diffractive scattering with the cluster model in Herwig". In: *Eur. Phys. J.* C77.3 (2017), p. 156. DOI: 10.1140/epjc/s10052-017-4727-7. arXiv: 1612.04701 [hep-ph].

[31] "Tuning and test of fragmentation models based on identified particles and precision event shape data DELPHI Collaboration". In: *Zeitschrift für Physik C Particles and Fields* 73.1 (1997), pp. 11–59. ISSN: 1431-5858. DOI: 10.1007/s002880050295. URL: https://doi.org/10.1007/s002880050295.

[32] *Herwig 7.0 Tuning plots.* https://herwig.hepforge.org/plots/herwig7.0/Rivet-LEP/DELPHI_1996_S3430090/index.html. Accessed: 2018-02-16.

[33] Maximilian Horzela. "Monte-Carlo simulations for cluster fission in Herwig (Monte-Carlo Simulationen zum Cluster Zerfall in Herwig)". Bachelor's Thesis. KIT, 2017.

[34] G.J. Alner et al. "The UA5 high energy pp simulation program". In: *Nuclear Physics B* 291 (1987), pp. 445 –502. ISSN: 0550-3213. DOI: https://doi.org/10.1016/0550-3213(87)90481-0. URL: http://www.sciencedirect.com/science/article/pii/0550321387904810.

[35] S. Jadach. "Rapidity generator for Monte-Carlo calculations of cylindrical phase space". In: *Computer Physics Communications* 9.5 (1975), pp. 297 –304. ISSN: 0010-4655. DOI: http://dx.doi.org/10.1016/0010-4655(75)90081-8. URL: http://www.sciencedirect.com/science/article/pii/0010465575900818.

[36] Andy Buckley et al. "Systematic event generator tuning for the LHC". In: *Eur. Phys. J.* C65 (2010), pp. 331–357. DOI: 10.1140/epjc/s10052-009-1196-7. arXiv: 0907.2973 [hep-ph].

[37] Andy Buckley et al. "Rivet user manual". In: *Comput. Phys. Commun.* 184 (2013), pp. 2803–2819. DOI: 10.1016/j.cpc.2013.05.021. arXiv: 1003.0694 [hep-ph].

[38] "Studies of QCD at e+e- centre-of-mass energies between 91 and 209 GeV". In: *The European Physical Journal C - Particles and Fields* 35.4 (2004), pp. 457–486. ISSN: 1434-6052. DOI: 10.1140/epjc/s2004-01891-4. URL: https://doi.org/10.1140/epjc/s2004-01891-4.

[39] A. Heister et al. "Inclusive production of the omega and eta mesons in Z decays, and the muonic branching ratio of the omega". In: *Phys. Lett.* B528 (2002), pp. 19–33. DOI: 10.1016/S0370-2693(02)01220-0. arXiv: hep-ex/0201012 [hep-ex].

[40] R. Barate et al. "Studies of Quantum Chromodynamics with the ALEPH detector". In: *Physics Reports* 294.1 (1998), pp. 1 –165. ISSN: 0370-1573. DOI: https://doi.org/10.1016/S0370-1573(97)00045-8. URL: http://www.sciencedirect.com/science/article/pii/S0370157397000458.

[41] D. Decamp et al. "Measurement of the charged particle multiplicity distribution in hadronic Z decays". In: *Physics Letters B* 273.1 (1991), pp. 181 –192. ISSN: 0370-2693. DOI: https://doi.org/10.1016/0370-2693(91)90575-B. URL: http://www.sciencedirect.com/science/article/pii/037026939190575B.

[42] P Abreu et al. "Measurement of inclusive Rho0, f0(980), f2(1270), Kstar02(1430) and fprime2(1525) production in Z0 decays". In: *Physics Letters B* 449.3 (1999), pp. 364 –382. ISSN: 0370-2693. DOI: https://doi.org/10.1016/S0370-2693(99)00105-7. URL: http://www.sciencedirect.com/science/article/pii/S0370269399001057.

[43] P. Abreu et al. "Strange baryon production in Z hadronic decays". In: *Zeitschrift für Physik C Particles and Fields* 67.4 (1995), pp. 543–553. ISSN: 1431-5858. DOI: 10.1007/BF01553980. URL: https://doi.org/10.1007/BF01553980.

[44] G. Abbiendi et al. "Measurement of event shape distributions and moments in e+ e- —> hadrons at 91-GeV - 209-GeV and a determination of alpha(s)". In: *Eur. Phys. J.* C40 (2005), pp. 287–316. DOI: 10.1140/epjc/s2005-02120-6. arXiv: hep-ex/0503051 [hep-ex].

[45] G. Abbiendi et al. "Multiplicities of pi0, eta, K0 and of charged particles in quark and gluon jets". In: *Eur. Phys. J.* C17 (2000), pp. 373–387. DOI: 10.1007/s100520000505. arXiv: hep-ex/0007017 [hep-ex].

[46] K. Ackerstaff et al. "Measurements of flavor dependent fragmentation functions in Z0 –> q anti-q events". In: *Eur. Phys. J.* C7 (1999), pp. 369–381. DOI: 10.1007/s100529901067. arXiv: hep-ex/9807004 [hep-ex].

[47] K. Ackerstaff et al. "Photon and light meson production in hadronic Z0 decays". In: *Eur. Phys. J.* C5 (1998), pp. 411–437. DOI: 10.1007/s100520050286. arXiv: hep-ex/9805011 [hep-ex].

[48] K. Ackerstaff et al. "Production of f(0)(980), f(2)(1270) and phi(1020) in hadronic Z0 decay". In: *Eur. Phys. J.* C4 (1998), pp. 19–28. DOI: 10.1007/s100520050183. arXiv: hep-ex/9802013 [hep-ex].

[49] K. Ackerstaff et al. "Spin alignment of leading K*(892)0 mesons in hadronic Z0 decays". In: *Phys. Lett.* B412 (1997), pp. 210–224. DOI: 10.1016/S0370-2693(97)01077-0. arXiv: hep-ex/9708022 [hep-ex].

[50] "Strange baryon production in hadronic Z0 decays". In: *Zeitschrift für Physik C Particles and Fields* 73.4 (1997), pp. 569–585. ISSN: 1431-5858. DOI: 10.1007/s002880050349. URL: https://doi.org/10.1007/s002880050349.

[51] "J/Ψ and Ψ' production in hadronic Z0 decays". In: *Zeitschrift für Physik C Particles and Fields* 70.2 (1996), pp. 197–209. ISSN: 1431-5858. DOI: 10.1007/s002880050096. URL: https://doi.org/10.1007/s002880050096.

[52] G Alexander et al. "Δ^{++} production in hadronic Z0 decays". In: *Physics Letters B* 358.1 (1995), pp. 162 –172. ISSN: 0370-2693. DOI: https://doi.org/10.1016/0370-2693(95)00935-E. URL: http://www.sciencedirect.com/science/article/pii/037026939500935E.

[53] R. Akers et al. "Measurement of the production rates of charged hadrons in e+e− annihilation at the Z0". In: *Zeitschrift für Physik C Particles and Fields* 63.2 (1994), pp. 181–195. ISSN: 1431-5858. DOI: 10.1007/BF01411010. URL: https://doi.org/10.1007/BF01411010.

[54] C. Amsler et al. "Review of Particle Physics". In: *Physics Letters B* 667.1 (2008). Review of Particle Physics, pp. 1 –6. ISSN: 0370-2693. DOI: https://doi.org/10.1016/j.physletb.2008.07.018. URL: http://www.sciencedirect.com/science/article/pii/S0370269308008435.

A Appendix

A.1 Weights of tunes

Table A.1: ALEPH_2004_S5765862 [38] (E_{CMS} = 91.2 GeV)

Observable	Weight gen.	Weight mult.	Observable	Weight gen.	Weight mult.
Thrust minor, m	1.0	-	Jet mass difference	1.0	-
Aplanarity, A	1.0	-	Oblateness, O	1.0	-
Sphericity, S	1.0	-			
Thrust, T	1.0	-	Heavy jet mass	1.0	-
Total jet broadening	1.0	-	Wide jet broadening	1.0	-
C-Parameter	1.0	-	Thrust major, M	1.0	-

Table A.2: ALEPH_2002_S4823664 [39]

Observable	Weight gen.	Weight mult.
η scaled momentum	1.0	-
ω scaled momentum	1.0	-

Table A.3: ALEPH_1996_S3486095 [40]

Observable	Weight gen.	Weight mult.	Observable	Weight gen.	Weight mult.
Sphericity, S (charged)	1.0	-	Aplanarity, A (charged)	1.0	-
1-Thrust, $1-T$ (charged)	1.0	-	Thrust minor, m (charged)	1.0	-
C parameter (charged)	1.0	-	Oblateness, $O = M - m$ (charged)	1.0	-
Scaled momentum, $x_p = \frac{\lvert p \rvert}{\lvert p_{\text{beam}} \rvert}$ (charged)	1.0	-	Rapidity w.r.t. thrust axes, y_T (charged)	1.0	-
In-plane p_T in GeV w.r.t. sphericity axes (charged)	1.0	-	Out-of-plane p_T in GeV w.r.t. sphericity axes (charged)	1.0	-
Log of scaled momentum, $\log\left(\frac{1}{x_p}\right)$ (charged)	1.0	-	Charged multiplicity distribution	1.0	-
Mean charged multiplicity	750	750	Mean charged multiplicity for rapidity $\lvert Y \rvert < 0.5$	750	750
Mean charged multiplicity for rapidity $\lvert Y \rvert < 1.0$	750	750	Mean charged multiplicity for rapidity $\lvert Y \rvert < 1.5$	750	750
Mean charged multiplicity for rapidity $\lvert Y \rvert < 2.0$	750	750			
Mean π^0 multiplicity	10	10	Mean η multiplicity	10	10
Mean η' multiplicity	10	10	Mean $K_S + K_L$ multiplicity	10	10
Mean ρ^0 multiplicity	10	10	Mean ρ(782) multiplicity	10	10
Mean ϕ multiplicity	10	10	Mean $K^{*\pm}$ multiplicity	10	10
Mean K^{*0} multiplicity	10	10	Mean Λ multiplicity	10	10
Mean Σ multiplicity	10	10	Mean Ξ multiplicity	10	10
Mean Σ(1385) multiplicity	10	10	Mean Ξ(1530) multiplicity	10	10
Mean $\Omega^{\mp}$	10	10			

Table A.4: ALEPH_1991_S2435284 [41]

Observable	Weight gen.	mult.
Total charged multiplicity	1.0	-

Table A.5: DELPHI_1999_S3960137 [42]

Observable	Weight gen.	mult.	Observable	Weight gen.	mult.
ρ^0 scaled momentum	1.0	-	$f^0(980)$ scaled momentum	1.0	-
$f_2(1270)$ scaled momentum	1.0		-		

Table A.6: DELPHI_1996_S3430090 [31]

Observable	Weight gen.	mult.	Observable	Weight gen.	mult.
In-plane $p_\perp$ in GeV w.r.t. thrust axes	1.0	-	Out-of-plane $p_\perp$ in GeV w.r.t. thrust axes	1.0	-
In-plane $p_\perp$ in GeV w.r.t. sphericity axes	1.0	-	Out-of-plane $p_\perp$ in GeV w.r.t. sphericity axes	1.0	-
Rapidity w.r.t. thrust axes, y_T	1.0	-	Rapidity w.r.t. sphericity axes, y_S	1.0	-
Scaled momentum $x_p = \frac{\lvert p \rvert}{p_{\mathrm{beam}}}$	1.0	-	Log of scaled momentum, $\log\left(\frac{1}{x_p}\right)$	1.0	-
Mean out-of-plane $p_\perp$ in GeV w.r.t. thrust axis vs. x_p	1.0	-	Mean $p_\perp$ in GeV vs. x_p	1.0	-
1-Thrust	1.0	-	Thrust major, M	1.0	-
Thrust minor, m	1.0	-	Oblateness, $O = M - m$	1.0	-
Sphericity, S	1.0	-	Aplanarity, A	1.0	-
Planarity, P	1.0	-	C parameter	1.0	-
D parameter	1.0	-	Heavy hemisphere masses, M_h^2/E_{vis}^2	1.0	-
Light hemisphere masses, M_l^2/E_{vis}^2	1.0	-	Difference in hemisphere masses, M_d^2/E_{vis}^2	1.0	-
Wide hemisphere broadening, B_{max}	1.0	-	Narrow hemisphere broadening, B_{min}	1.0	-
Total hemisphere broadening, B_{sum}	1.0	-	Difference in hemisphere broadening, B_{diff}	1.0	-
Energy-energy scaled momentum, EEC	1.0	-	Asymmetry of the energy-energy correlation, AAEC	1.0	-
Mean charged multiplicity	750	750	Mean π^+/π^- multiplicity	10	10
Mean π^0 multiplicity	10	10	Mean K^+/K^- multiplicity	10	10
Mean K^0 multiplicity	10	10	Mean η multiplicity	10	10
Mean η' multiplicity	10	10	Mean D^+ multiplicity	10	10
Mean D^0 multiplicity	10	10	Mean $B^+/B^-/B^0$ multiplicity	10	10
Mean $f_0(980)$ multiplicity	10	10	Mean ρ multiplicity	10	10
Mean $K^*(892)^+/K^*(892)^-$ multiplicity	10	10	Mean $K^*(892)^0$ multiplicity	10	10
Mean ϕ multiplicity	10	10	Mean $D^*(2010)^+/D^*(2010)^-$ multiplicity	10	10
Mean $f_2(1270)$ multiplicity	10	10	Mean $K_2^*(1430)^0$ multiplicity	10	10
Mean p multiplicity	10	10	Mean Λ^0 multiplicity	10	10
Mean Ξ^- multiplicity	10	10	Mean Ω^- multiplicity	10	10
Mean $\Delta(1232)^{++}$ multiplicity	10	10	Mean $\Sigma(1385)^+/\Sigma(1385)^-$ multiplicity	10	10
Mean $\Xi(1530)^0$ multiplicity	10	10	Mean Λ_b^0 multiplicity	10	10

Table A.7: DELPHI_1995_S3137023[43]

Observable	Weight gen.	mult.
Ξ^- scaled momentum	1.0	-
$\Sigma^\pm(1385)$ scaled momentum	1.0	-

Table A.8: OPAL_2004_S6132243[44]

Observable	Weight gen.	mult.	Observable	Weight gen.	mult.
Thrust, $1 - T$, at 91 GeV	1.0	-	Heavy hemisphere mass, M_H, at 91 GeV	1.0	-
C parameter at 91 GeV	1.0	-	Total hemisphere broadening, B_{sum}, at 91 GeV	1.0	-
Wide hemisphere broadening, B_{max}, at 91 GeV	1.0	-			
Thrust major, T_{maj}, at 91 GeV	1.0	-	Thrust minor, T_{min}, at 91 GeV	1.0	-
Aplanarity, A, at 91 GeV	1.0	-	Sphericity, S, at 91 GeV	1.0	-
Oblateness, O, at 91 GeV	1.0	-	Light hemisphere mass, M_L, at 91 GeV	1.0	-
Narrow hemisphere broadening, B_{min}, at 91 GeV	1.0	-	D parameter at 91 GeV	1.0	-
Moments of $1 - T$ at 91 GeV	1.0	-	Moments of M_H at 91 GeV	1.0	-
Moments of C at 91 GeV	1.0	-	Moments of B_{sum} at 91 GeV	1.0	-
Moments of B_{max} at 91 GeV	1.0	-	Moments of y_{23} at 91 GeV	1.0	-
Moments of T_{maj} at 91 GeV	1.0	-	Moments of T_{min} at 91 GeV	1.0	-
Moments of S at 91 GeV	1.0	-	Moments of O at 91 GeV	1.0	-
Moments of M_L at 91 GeV	1.0	-	Moments of B_{min} at 91 GeV	1.0	-

Table A.9: OPAL_2000_S4418603 [45]

Observable	Weight	
	gen.	mult.
K^0 scaled momentum	1.0	-

Table A.10: OPAL_1998_S3780481 [46]

Observable	Weight		Observable	Weight	
	gen.	mult.		gen.	mult.
uds scaled momentum	1.0	-	c events scaled momentum	1.0	-
b events scaled momentum	1.0	-	All events scaled momentum	1.0	-
uds events $\ln(1/x_p)$	1.0	-	c events $\ln(1/x_p)$	1.0	-
b events $\ln(1/x_p)$	1.0	-	All events $\ln(1/x_p)$	1.0	-
uds events mean charged multiplicity	750	750	c events mean charged multiplicity	750	750
b events mean charged multiplicity	750	750	All events mean charged multiplicity	750	750

Table A.11: OPAL_1998_S3749908 [47]

Observable	Weight		Observable	Weight	
	gen.	mult.		gen.	mult.
Photon scaled momentum	1.0	-	Photon scaled momentum, $\ln(1/x_p)$	1.0	-
π^0 scaled momentum	1.0	-	π^0 scaled momentum, $\ln(1/x_p)$	1.0	-
η scaled momentum	1.0	-	η scaled momentum, $\ln(1/x_p)$	1.0	-
$\rho^\pm$ scaled momentum	1.0	-	$\rho^\pm$ scaled momentum, $\ln(1/x_p)$	1.0	-
ω scaled momentum	1.0	-	ω scaled momentum, $\ln(1/x_p)$	1.0	-
η' scaled momentum	1.0	-	η' scaled momentum, $\ln(1/x_p)$	1.0	-
$a_0^\pm$ scaled momentum	1.0	-	$a_0^\pm$ scaled momentum, $\ln(1/x_p)$	1.0	-

Table A.12: OPAL_1998_S3702294 [48]

Observable	Weight		Observable	Weight	
	gen.	mult.		gen.	mult.
$f_0(980)$ scaled momentum	1.0	-	$f_2(1270)$ scaled momentum	1.0	-
$\phi(1020)$ scaled momentum	1.0	-			

Table A.13: OPAL_1997_S3608263 [49]

Observable	Weight	
	gen.	mult.
K^{*0} scaled momentum	1.0	-

Table A.14: OPAL_1997_S3396100 [50]

Observable	Weight		Observable	Weight	
	gen.	mult.		gen.	mult.
Λ^0 scaled momentum	1.0	-	Λ^0 scaled momentum, $\ln(1/x_p)$	1.0	-
Ξ^- scaled momentum	1.0	-	Ξ^- scaled momentum, $\ln(1/x_p)$	1.0	-
$\Sigma^+(1385)$ scaled momentum	1.0	-	$\Sigma^+(1385)$ scaled momentum, $\ln(1/x_p)$	1.0	-
$\Sigma^-(1385)$ scaled momentum	1.0	-	$\Sigma^-(1385)$ scaled momentum, $\ln(1/x_p)$	1.0	-
$\Xi^0(1530)$ scaled momentum	1.0	-	$\Xi^0(1530)$ scaled momentum, $\ln(1/x_p)$	1.0	-
$\Lambda^0(1520)$ scaled momentum	1.0	-	$\Lambda^0(1520)$ scaled momentum, $\ln(1/x_p)$	1.0	-

Table A.15: OPAL_1996_S3257789 [51]

Observable	Weight		Observable	Weight	
	gen.	mult.		gen.	mult.
J/Ψ scaled momentum	1.0	-	J/Ψ Multiplicity	10	10
Ψ' Multiplicity	10	10			

Table A.16: OPAL_1995_S3198391 [52]

Observable	Weight	
	gen.	mult.
Δ^{++} scaled momentum	1.0	-

Table A.17: OPAL_1994_S2927284 [53]

Observable	Weight		Observable	Weight	
	gen.	mult.		gen.	mult.
$\pi^{\pm}$ momentum	1.0	-	$K^{\pm}$ momentum	1.0	-
$p, \bar{p}$ momentum	1.0	-			

Table A.18: PDG_HADRON_MULTIPLICITIES [54]

Observable	Weight		Observable	Weight	
	gen.	mult.		gen.	mult.
Mean π^+ multiplicity	10	10	Mean π^0 multiplicity	10	10
Mean K^+ multiplicity	10	10	Mean K^0 multiplicity	10	10
Mean η multiplicity	10	10	Mean $\eta'(958)$ multiplicity	10	10
Mean D^+ multiplicity	10	10	Mean D^0 multiplicity	10	10
Mean D_s^+ multiplicity	10	10	Mean B^+, B_d^0 multiplicity	10	10
Mean B_u^+ multiplicity	10	10	Mean B_s^0 multiplicity	10	10
Mean $f_0(980)$ multiplicity	10	10	Mean $a_0^+(980)$ multiplicity	10	10
Mean $\rho^0(770)$ multiplicity	10	10	Mean $\rho^+(770)$ multiplicity	10	10
Mean $\omega(782)$ multiplicity	10	10	Mean $K^{*+}(892)$ multiplicity	10	10
Mean $K^{*0}(892)$ multiplicity	10	10	Mean $\phi(1020)$ multiplicity	10	10
Mean $D^{*+}(2010)$ multiplicity	10	10	Mean $D_s^{*+}(2112)$ multiplicity	10	10
Mean B^* multiplicity	10	10	Mean $J/\Psi(1S)$ multiplicity	10	10
Mean $\Psi(2S)$ multiplicity	10	10	Mean $\Upsilon(1S)$ multiplicity	10	10
Mean $f_1(1285)$ multiplicity	10	10	Mean $f_1(1420)$ multiplicity	10	10
Mean $\chi_{\mathrm{cl}}(3510)$ multiplicity	10	10	Mean $f_2(1270)$ multiplicity	10	10
Mean $f_2'(1525)$ multiplicity	10	10	Mean $K_2^{*0}(1430)$ multiplicity	10	10
Mean B^** multiplicity	10	10	Mean D_{s1}^+ multiplicity	10	10
Mean D_{s2}^+ multiplicity	10	10	Mean p multiplicity	10	10
Mean Λ multiplicity	10	10	Mean Σ^0 multiplicity	10	10
Mean Σ^- multiplicity	10	10	Mean Σ^+ multiplicity	10	10
Mean $\Sigma^\pm$ multiplicity	10	10	Mean Ξ^- multiplicity	10	10
Mean $\Delta^{++}(1232)$ multiplicity	10	10	Mean $\Sigma^-(1385)$ multiplicity	10	10
Mean $\Sigma^+(1385)$ multiplicity	10	10	Mean $\Sigma^\pm(1385)$ multiplicity	10	10
Mean $\Xi^0(1530)$ multiplicity	10	10	Mean Ω^- multiplicity	10	10
Mean Λ_c^+ multiplicity	10	10	Mean Λ_b^0 multiplicity	10	10
Mean $\Lambda(1520)$ multiplicity	10	10			

Acknowledgements

First of all I thank my supervisor PD Dr. Stefan Gieseke for the opportunity to join his working group and work on this interesting topic. Furthermore I would like to thank him for continuous support throughout the time of this work and open ears whenever there were questions and problems arising. I am also grateful for the opportunity to join the MCnet Meeting in Karlsruhe.
Next I would like to thank Prof. Dr. Dieter Zeppenfeld who agreed to be the second reviewer of this thesis.
Special thanks to Patrick Kirchgaesser for the many times he gave me advice throughout the work on this thesis, being always helpful whenever there were problems or questions and specifically for proofreading this thesis.
Additionally I would like to thank Emma Simpson Dore for also proofreading this thesis and for her support and welcome distraction not just in stressful times during the last months of the work.
Furthermore thanks to Stefan Maier and Michael Raumer for proofreading this thesis and being very helpful throughout the course of our studies.
Thanks to all members of the Institute of Theoretical Physics for the productive and fun atmosphere at the institute. I thoroughly enjoyed working at the ITP this past year.
Last but not least I would like to thank my mother for her continuous support throughout the years of my studies. Without her support it would have been impossible for me to study in the first place.